iScience

CellPress
OPEN ACCESS

Article

Protective role of seleno-amino acid against IBD via ferroptosis inhibition in enteral nutrition therapy

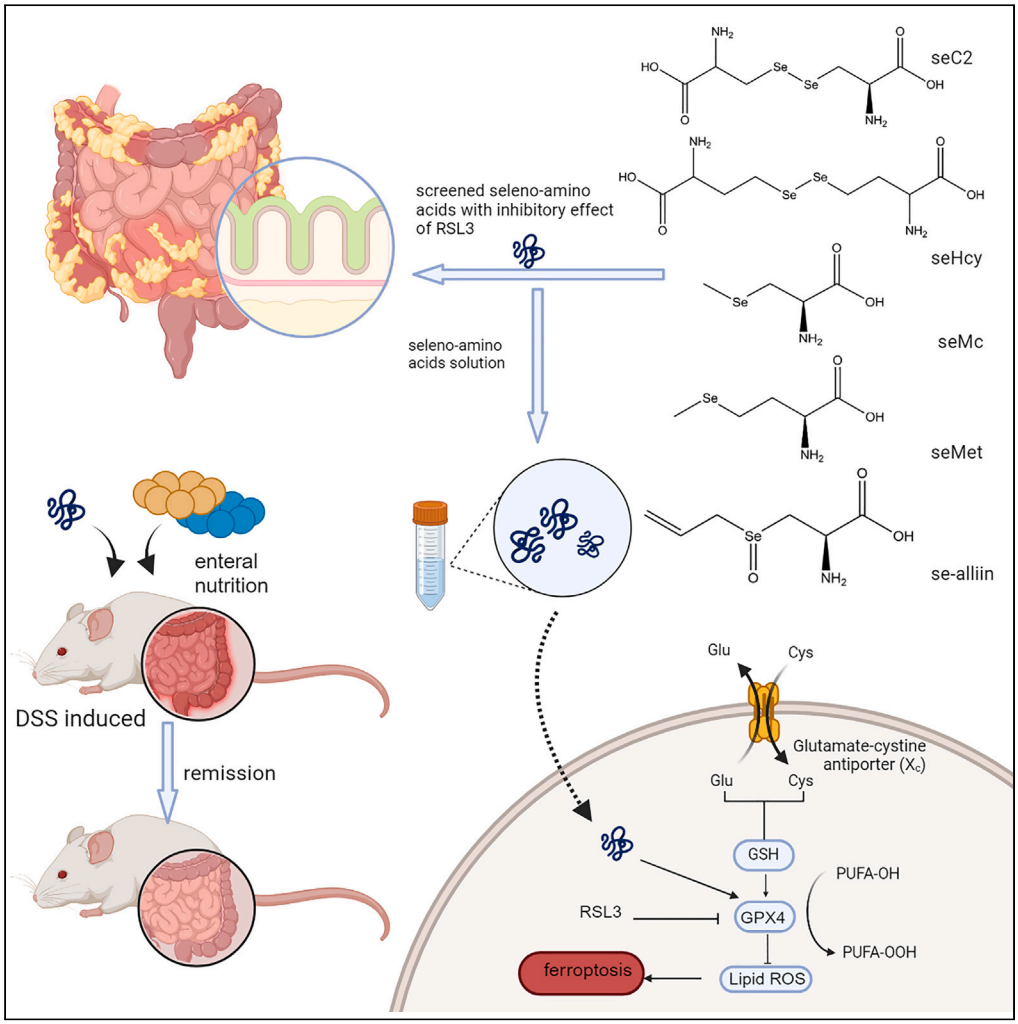

Shuchen Huangfu, Jie Zheng, Jiashuai He, Jin Liao, Haiping Jiang, Hua Zhou, Jinghua Pan

qwwer@139.com (H.J.)
zhouhua5460@jnu.edu.cn (H.Z.)
huajanve@foxmail.com (J.P.)

Highlights

Natural seleno-amino acids protect the intestinal barrier by GPX4/GSH antioxidant

We investigated the relationships among seleno-amino acids, GPX4, and IBD

seMc treatment alleviated decreased GPX4 expression in ferroptosis-induced cells

seMc with enteral nutrition therapy alleviated IBD-related intestinal symptoms

Huangfu et al., iScience 27, 110494
September 20, 2024
https://doi.org/10.1016/j.isci.2024.110494

iScience

CellPress
OPEN ACCESS

Article

Protective role of seleno-amino acid against IBD via ferroptosis inhibition in enteral nutrition therapy

Shuchen Huangfu,[1,3] Jie Zheng,[2,3] Jiashuai He,[1] Jin Liao,[2] Haiping Jiang,[1,*] Hua Zhou,[2,*] and Jinghua Pan[1,4,*]

SUMMARY

The interplay between intestinal barrier degradation and trace element insufficiency worsens inflammatory bowel disease (IBD). Selenium (se) is essential for glutathione peroxidase 4 (GPX4) synthesis, which protects against intestinal epithelial cell injury in IBD. However, malnutrition and malabsorption limit the availability of dietary selenium. This study investigated the protective effects of naturally occurring seleno-amino acids on the intestinal barrier in an IBD animal model by promoting GPX4 synthesis. L-se-methylselenocystine (seMc) supplementation reversed decreased GPX4 expression levels, alleviated glutathione depletion and scavenged reactive oxygen species *in vitro*. *In vivo*, enteral nutrition combined with seMc protected the intestinal barrier and alleviated IBD-related symptoms by inhibiting ferroptosis and reversing lipid peroxidation in epithelial cells while reducing immune cell infiltration. Our findings suggest that seleno-amino acid-based nutritional formulations may provide a basis for nutritional support to alleviate complex cycles between intestinal barrier damage and malnutrition in IBD patients.

INTRODUCTION

Inflammatory bowel disease (IBD) is a common chronic idiopathic disease of the digestive tract with two main forms: Chron's disease (CD) and ulcerative colitis (UC).[1] The clinical symptoms of IBD include long-term recurrent abdominal pain, diarrhea, bloody stools, gastrointestinal perforation, and other extra-intestinal symptoms. Malnutrition is a serious complication of IBD, mainly caused by insufficient nutrient intake and loss due to intestinal barrier damage.[2,3] A previous study demonstrated that malnutrition was a spontaneous consequence of IBD and was detectable in 65–75% and 18–62% of patients with CD and ulcerative colitis (UC), respectively.[4] Malnutrition can significantly increase the risk of adverse outcomes in IBD. Previous studies have shown that compared with non-malnourished IBD patients, malnourished patients have longer hospital stays, increased perioperative risks, and higher mortality.[5] Malnutrition causes a disordered gut microbial composition, which may alter homeostasis and cause a dysregulated state, triggering a vicious inflammatory response cycle.[6] Thus, dietary support for patients with IBD is a critical but challenging issue. Although enteral nutrition therapy (ENT) is the preferred nutritional support for patients with IBD, which is more consistent with the way of nutrient absorption in physiological state, IBD involving the entire digestive tract has limited tolerance to nutritional therapy, rendering it inefficient. The intestinal mechanical barrier is a complete and closely connected intestinal mucosal epithelial structure comprising intestinal epithelial cells that help absorb nutrients and prevent harmful substances from penetrating the intestinal mucosa.[7] In IBD, intestinal epithelial cell death disrupts the integrity of the intestinal mechanical barrier, allowing pathogenic invasion and impairing nutrient intake.[8] Therefore, although challenging, intestinal barrier repair is urgently required for effective nutritional IBD treatments.

The clinical treatments to repair intestinal barrier function are limited and prone to drug dependence. Therefore, alternative remedies are in high demand. During mucosal inflammation, intestinal epithelioid cells (IECs) produce excess reactive oxygen species (ROS), which injures cytoskeletal proteins and alters tight junctions and epithelial permeability in IECs, contributing to barrier disruption.[9] Recent studies have found that ferroptosis is involved in the process of IECs death in IBD.[10] Ferroptosis is an iron-dependent programmed cell death process with characteristics that differ from those of other cell death types at the cellular morphological, biochemical, and genetic levels.[11] The two main biochemical features of ferroptosis are related, iron accumulation and lipid peroxidation. In ferroptosis, divalent iron ions accumulate in cells and cause the Fenton reaction, which generates hydroxyl radicals that bind with polyunsaturated fatty acids in the cell and plasma membranes to generate a significant amount of lipid ROS, causing cell death.[12] Previous studies have found that iron chelators can effectively reduce ROS production and improve intestinal symptoms in IBD.[13] The increase of dietary iron intake also increases the risk of IBD.[14,15] In dextran sulfate sodium (DSS)-induced mouse model, ferroptosis inhibitor can reduce the disease activity score of IBD mice.[10,16] Previous

[1]Department of General Surgery, the First Affiliated Hospital of Jinan University, Guangzhou 510632, China
[2]Department of Food Science and Engineering, Jinan University, Guangzhou 510632, China
[3]These authors contributed equally
[4]Lead contact
*Correspondence: qwwer@139.com (H.J.), zhouhua5460@jnu.edu.cn (H.Z.), huajanve@foxmail.com (J.P.)
https://doi.org/10.1016/j.isci.2024.110494

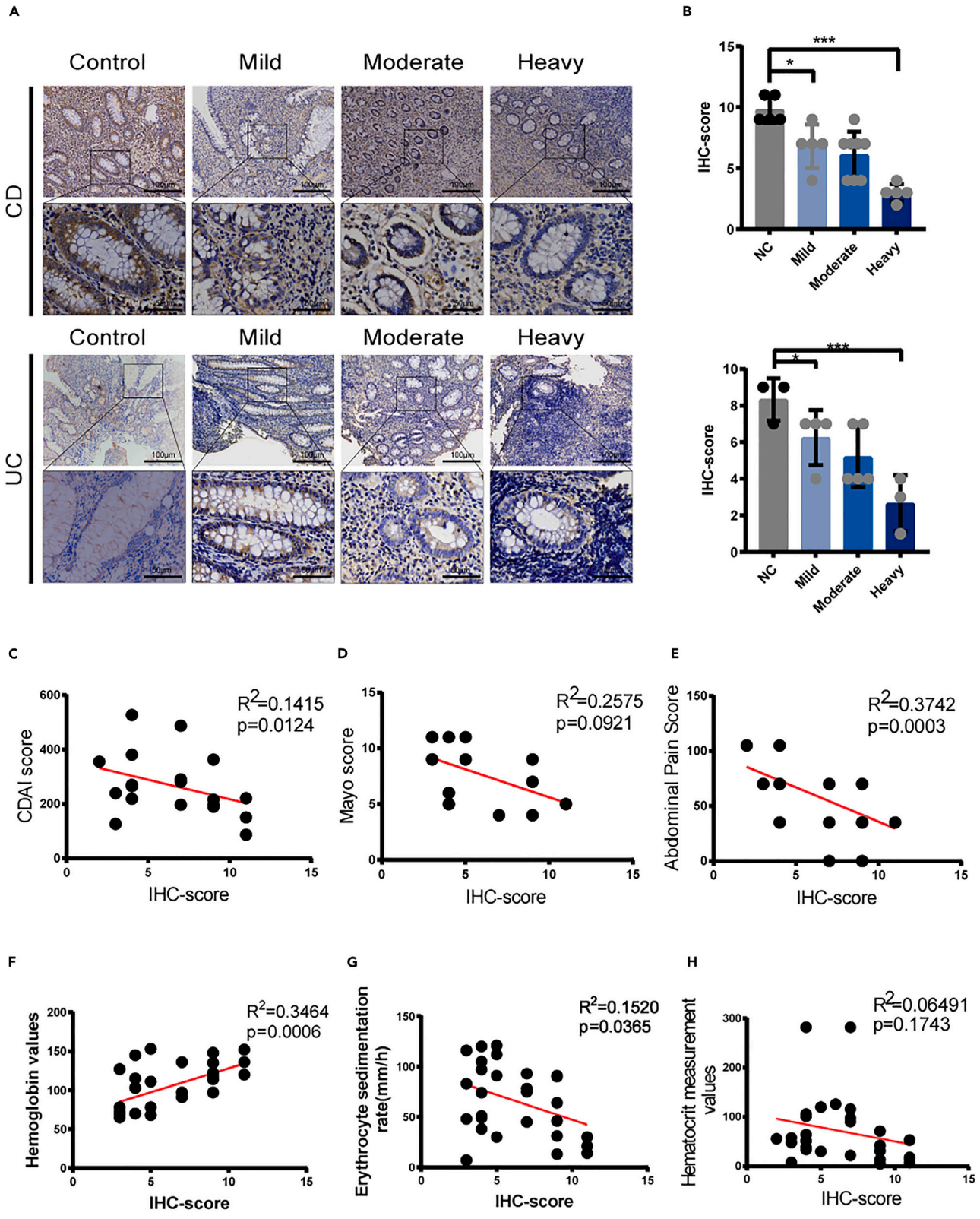
A
Control
Mild
Moderate
Heavy
CD
UC
B
IHC-score
NC
Mild
Moderate
Heavy
C
CDAI score
R2=0.1415
p=0.0124
IHC-score
D
Mayo score
R2=0.2575
p=0.0921
IHC-score
E
Abdominal Pain Score
R2=0.3742
p=0.0003
IHC-score
F
Hemoglobin values
R2=0.3464
p=0.0006
IHC-score
G
Erythrocyte sedimentation rate(mm/h)
R2=0.1520
p=0.0365
IHC-score
H
Hematocrit measurement values
R2=0.06491
p=0.1743
IHC-score

Figure 1. The expression level of GPX4 in colonic epithelium is correlated with clinical IBD disease activity

(A) IHC of GPX4 expression in colonic epithelial tissue from IBD patients; (B) quantification of GPX4 expression in colonic epithelial tissue from IHC (data are represented as mean ± SEM); (C) correlation between IHC-score and CDAI(R^2 = 0.1415, p = 0.0124); (D) correlation between IHC-score and Mayo score (R^2 = 0.2575, p = 0.0921); (E) correlation between IHC-score and abdominal pain score(R^2 = 0.0.284, p = 0.0118); (F) correlation between IHC-score and hemoglobin values(R^2 = 0.3406, p = 0.0139); (G) correlation between IHC-score and eythrocyte sedimentation rate(R^2 = 0.0701, p = 0.4595); (H) correlation between IHC-score and Hematocrit measurement(R^2 = 0.05919, p = 0.2035); *, **, and *** indicate p values less than 0.05, 0.01, and 0.001, respectively.

studies on genetics have found significant changes in ferroptosis-related genes in IBD patients.[17] These findings provide suggestive evidence for the presence of ferroptosis in IBD.

Among the various regulatory pathways of ferroptosis, the glutathione-dependent pathway has been identified as the classical one. The expression level of glutathione peroxidase 4 (GPX4), which is the key regulatory protein of ferroptosis, was found to be changed in the colon tissues of IBD patients. Decreased glutathione (GSH) concentrations from decreased GPX4 levels regulate intracellular lipid peroxidation and trigger ferroptosis.[18] GPX4 is one of the glutathione peroxidases (GPX) families, which was the first selenoprotein family to be discovered and is highly sensitive to changes in the utilization of seleno-amino acids.[19] Seleno-amino acids not only play an antioxidant role by directly acting as antioxidants, but also participate in the synthesis of other Se-dependent antioxidants as Se sources.[20] Studies have found that intestinal epithelial cells can take up selenoamino acids from intestinal contents and participate in the synthesis of selenoproteins.[21]

Given the relationships among GPX4, Se, ferroptosis, and IBD, we hypothesized that GPX4 expression levels affect IBD via ferroptosis and that organic Se would improve the intestinal barrier and, thus, IBD symptoms. Therefore, we investigated the associations among GPX4 expression, seleno-amino acids, and the IBD status using *in vitro* and *in vivo* studies to provide foundational evidence for an Se-based nutritional support scheme.

RESULTS

GPX4 expression in the colonic epithelium correlates with the clinical IBD disease status

This study included clinical samples from 18 to 12 patients with pathologically confirmed CD and UC, respectively; Tables S1 and S2 present the CD and UC clinical grades based on the modified Mayo scores. According to the 2023 revised ECCO guidelines on Inflammatory Bowel Disease and Malignancies, the Clinical Disease Activity Index (CDAI) score is based on various patient characteristics, including stool frequency, abdominal pain, general health, clinical presentation, diarrhea, medication use, presence of abdominal mass, hematocrit (HCT), and weight loss. A total score below 150 indicates remission; scores above 150 indicate activity with mild activity between 150 and 220, moderate activity between 220 and 450, and severe activity above 450. The modified Mayo score includes subscores for frequency of stools, blood in the stool, endoscopic evaluation, and overall physician evaluation. A total score of $\leq$2 with no individual subscore >1 indicates clinical remission; scores ranging from 3 to 5 indicate mild activity followed by moderate activity for scores ranging from 6 to 10 and severe activity for scores of 11–12.[22] Immunohistochemical (IHC) staining showed higher GPX4 expression in the colonic epithelium than in normal colonic tissues, gradually decreasing as the IBD disease severity increased (Figures 1A and 1B). Furthermore, the GPX4 expression level negatively correlated with the CDAI and abdominal pain scores (R^2 = 0.141 and 0.284, respectively, $p < 0.05$; Figures 1C and 1E) but positively correlated with the hemoglobin level in patients with IBD (R^2 = 0.3406, $p < 0.05$; Figure 1F). Other clinical indicators used to determine the clinical IBD grading, including the Mayo score, erythrocyte sedimentation index, and hematocrit, negatively correlated with the GPX4 expression in the colonic epithelium, but the difference was insignificant ($p > 0.05$; Figures 1D, 1G, and 1H).

Seleno-amino acids inhibit RSL3-induced cell death

The protective effects of five seleno-amino acids (selenohomocysteine [seHcy], Selenocysteine [seC2], L-se-Methylselenocysteine [seMc], Selenomethionine [seMet], and se-alliin) against RSL3-induced cell death in Caco-2 cells were explored; Figure 2A presents their chemical structures. RSL3 (i.e., [1S,3R]-RSL3) covalently binds GPX4, inactivating it, which causes intracellular peroxide accumulation, ferroptosis, and cell death.

Seleno-amino acids inhibited RSL3-induced Caco-2 cell death; a 50 μM treatment with all the seleno-amino acids significantly mitigated RSL3-induced cell death compared to the control group (Figure 2B), but seMc had the greatest protective effect. The average RSL3-induced cell death rate was 36.5%, which decreased to 1.6% after seMc treatment. seHcy and seC2 also dose-dependently inhibited RSL3-induced cell death, ranging from 18.4 to 37.6% and 13.0–37.3%, respectively. However, seMc and seMet inhibited RSL3-induced cell death at concentrations of 50 μM and above.

Se concentrations in the intracellular fluid were measured using inductively coupled plasma-mass spectrometry (ICP-MS), demonstrating that Se concentration changes in the intracellular fluid differed when 50 μM of seleno-amino acids were added to the cell culture medium. The intracellular Se concentration in seMc group was 0.013 μM, which was significantly higher than those in the seHcy (0.0005 μM), seC2 (0.003 μM), seMet (0.003 μM), and se-allicin (0.0006 μM) groups (Figure 2D). In addition, seMc had the highest absorption rate and best protective effect against RSL3-induced cell death. Therefore, seMc was selected for further studies.

Brightfield plots visually demonstrated that seMc protected colon epithelial cells from RSL3-induced cell membrane fragmentation and cell death; obvious cell death was not observed in Caco-2 cells treated with seMc alone, indicating that seMc was not cytotoxic at the experimental concentration (Figure 2C). To verify the protective effects of seMc against cell death, the survival rates of colon epithelium-derived

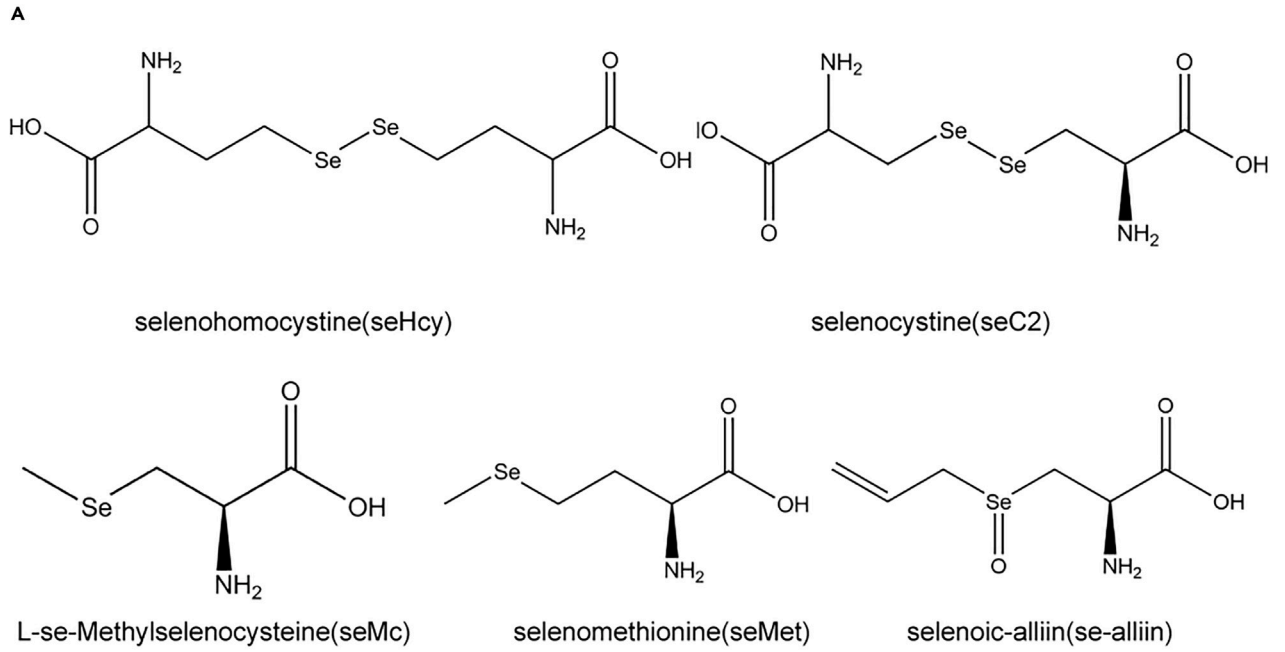
A
selenohomocystine(seHcy)
selenocystine(seC2)
L-se-Methylselenocysteine(seMc)
selenomethionine(seMet)
selenoic-alliin(se-alliin)

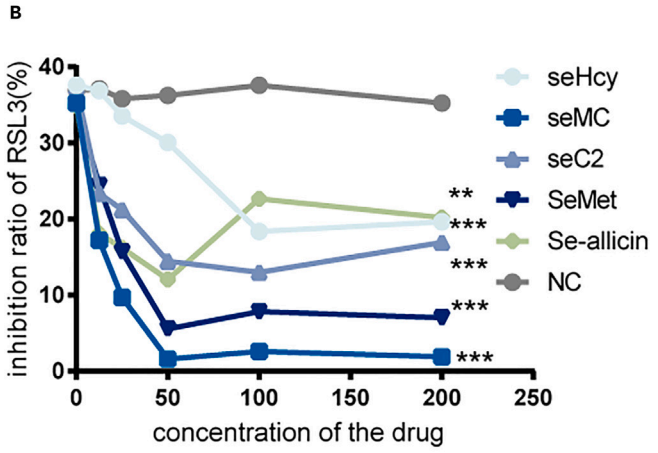
B
inhibition ratio of RSL3(%)
concentration of the drug
seHcy
seMC
seC2
SeMet
Se-allicin
NC

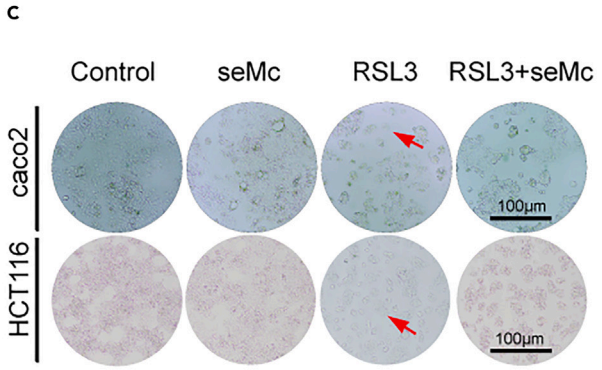
C
Control
seMc
RSL3
RSL3+seMc
caco2
HCT116
100μm

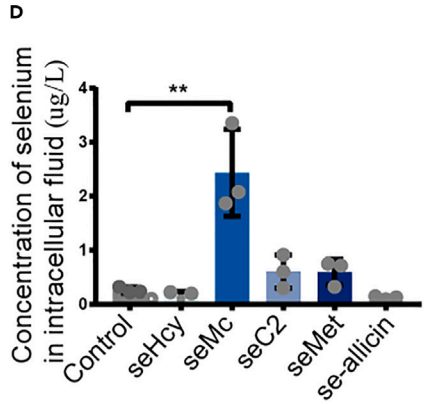
D
Concentration of selenium in intracellular fluid (ug/L)
Control
seHcy
seMc
seC2
seMet
se-allicin

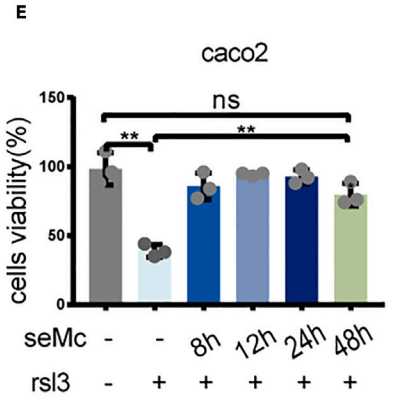
E
caco2
cells viability(%)
seMc
rsl3
8h
12h
24h
48h

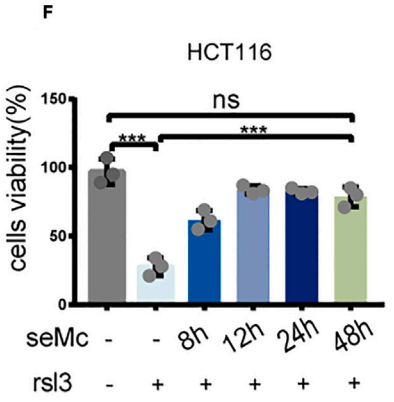
F
HCT116
cells viability(%)
seMc
rsl3
8h
12h
24h
48h

Figure 2. se-rich amino acids inhibited RSL3-induced ferroptosis

(A) Chemical formulae for five se-rich amino acids; (B) inhibition rate of the induction of RSL3 by different concentrations of se-rich amino acids; (C) bright-field images of cell morphology after seMc/RSL3 treatment, ruptured cells are marked by red arrows (scale bars: 100μm); (D) intracellular se content after treatment with five se-rich amino acids measured by Lcy-ms (data are represented as mean ± SEM); (E) viability of caco2 cells treated with seMc/RSL3 for 8 h,12 h,24 h, and 48 h, respectively (data are represented as mean ± SEM); (F) viability of HCT116 cells treated with seMc/RSL3 for 8 h,12 h,24 h, and 48 h, respectively (data are represented as mean ± SEM). *, **, and *** indicate *p* values less than 0.05, 0.01, and 0.001, respectively.

Caco-2 and HCT116 cells treated with RSL3 at different time points were examined. Compared with the RSL3-only group, the cell survival rate significantly increased after 8 h of seMc intervention, peaking after 12 h (Figures 2E and 2F).

Seleno-amino acids-GPX4 interactions

The results of molecular docking for seleno-amino acids binding to GPX4 protein are shown as following. Based on the results of previous studies, the five seleno-amino acids we employed had differential effects on RSL3-induced cell activity, so GPX4 was selected as the target protein which is the core protein related with ferroptosis to deeply investigate the interaction between seleno-amino acids and it. As shown in Figures 3A–3E, the amino terminus of seleno-amino acids formed an efficient hydrogen bond with GPX4 protein, but their binding sites, number of hydrogen bonds and binding affinity are different (Figure S1). seHcy binds efficiently to the GPX4 active pocket by forming a hydrogen bond between Lcy135 and Met129 of GPX4 (Figure 3A); seC2 formed hydrogen bonds with ARG152, ARG127, Lys135, and Met129 (Figure 3B); seMc formed hydrogen bonds with Lys135, ARG152, and MET129 (Figure 3C); seMet formed hydrogen bonds with SER44, GLN45, and GLY84 of GPX4 protein (Figure 3D), while se-alliin band with Lys121 and GLY110 (Figure 3E).

seMc inhibits RSL3-induced ferroptosis in colonic epithelial cells

To verify whether seMc elicited protective effects on epithelial cells via ferroptosis inhibition, we investigated the morphological structure of the mitochondria in seMc- or RSL3-treated cells using transmission electron microscopy (Figure 4A). Mitochondrial shrinkage, membrane thickening, and cristae reduction occurred in RSL3-treated cells compared to the control cells.

Fe^{2+} accumulation is another prominent feature of ferroptosis; therefore, we measured the Fe^{2+} content in cells after seMc intervention using immunofluorescence. The Fe^{2+} fluorescence intensity was significantly higher in the RLS3 group than in the control group but decreased after seMc treatment (Figures 4B and 4E). Furthermore, the RSL3 and seMc treatments significantly affected the expression of key proteins in the ferroptotic pathway (Figure 4C), the most obvious being GPX4, with considerably decreased expression in RSL3-treated cells but increased expression, returning to the level of the control group, after seMc intervention. Moreover, we found seMc increased nuclear factor erythroid 2-related factor 2 (NRF2) expressions in RSL3-treated caco2 cells, but decreased downstream heme oxygenase-1 (HO-1) protein expression (Figures S2A–S2C). Figure 4D presents the Inden value of GPX4 detected by western blot. The GSH concentration was significantly lower in the RSL3 group than in the control group, which was partially restored after seMc treatment (Figure 4F). seMc treatment also decreased the Malondialdehyde (MDA) level, a lipid peroxidation marker closely associated with iron toxicity, in RSL3-treated cells (Figure 4G). Furthermore, we amined the ability of seMc to clear RSL3-induced ROS production. Compared with control group, cytosolic ROS were increased after RSL3 treatment for 12h, 24h, 36h, 48h, and 72h, respectively. They were disrupted by the administration of seMc compare with RSL3 treatment alone (Figure 4H). The RSL3-induced lipid peroxidation was scavenge in group of seMc-treated (99.55%, 103.3%, 105.9%, 105.3%, and 105.3%, respectively). (Figure 4I). These data suggest that seMc might inhibit RSL3-triggered cell death by decreasing lipid peroxidation.

seMc alleviates LPS-induced epithelial cell injury by inhibiting ferroptosis

Many studies have shown that Lipopolysaccharide (LPS) can induce ferroptosis and inflammation *in vivo* and *in vitro*, therefore, our study further evaluated the inhibitory effect of seMc on ferroptosis induced by LPS. Caco-2 cells were treated with LPS to generate an inflammatory cell injury model, resulting in different degrees of morphological changes to the mitochondria, which returned to normal after seMc treatment (Figure 5A). Similarly, seMc reversed the LPS-induced decrease in GPX4 expression, resulting in significantly different expression levels between the LPS and LPS + seMc groups ($p < 0.05$; Figures 5C and 5D). In addition, we detected the expression of ferroptosis-related protein NRF2 and HO-1, and results indicated that the expression of NRF2 was increased in RSL3-induced caco2 cells after treated with seMc and the expression of HO-1 was decreased (Figures S3A–S3C).

Immunofluorescence indicated that LPS treatment increased the Fe^{2+} content by approximately 2-fold, but seMc treatment increased the content to the same level as the control group (Figures 5B and 5E). Intracellular GSH and MDA concentrations were also measured to verify that seMC alleviates LPS-induced cell damage by inhibiting ferroptosis. seMc significantly inhibited the LPS-induced increase in the GSH concentration ($p < 0.05$; Figure 5F). The MDA concentrations of LPS and LPS + seMc groups were 7.83 μmol/gprot and 5.11 μmol/gprot, respectively (Figure 5G). Flow cytometric analysis of cytosolic ROS after LPS stimulation for 24 h showed that they were scavenge by the administration of seMc, compare with LPS treatment alone, which was were statistically significant (Figure 5H). To investigate the role of ferroptosis in LPS-induced cell injury, lipid perdoxidation were assayed. The results shown that it increased with LPS intervention time (99.5%, 118.5%, 132.9%, 130.2%, 122.1%, respectively, stimulated for 12 h, 24 h, 36 h, 48 h, and 72 h), and it were disrupted by treatment of seMc (100.1%, 104.8%, 106.6%, 105.2% and 105.0%, respectively) (Figure 5I).

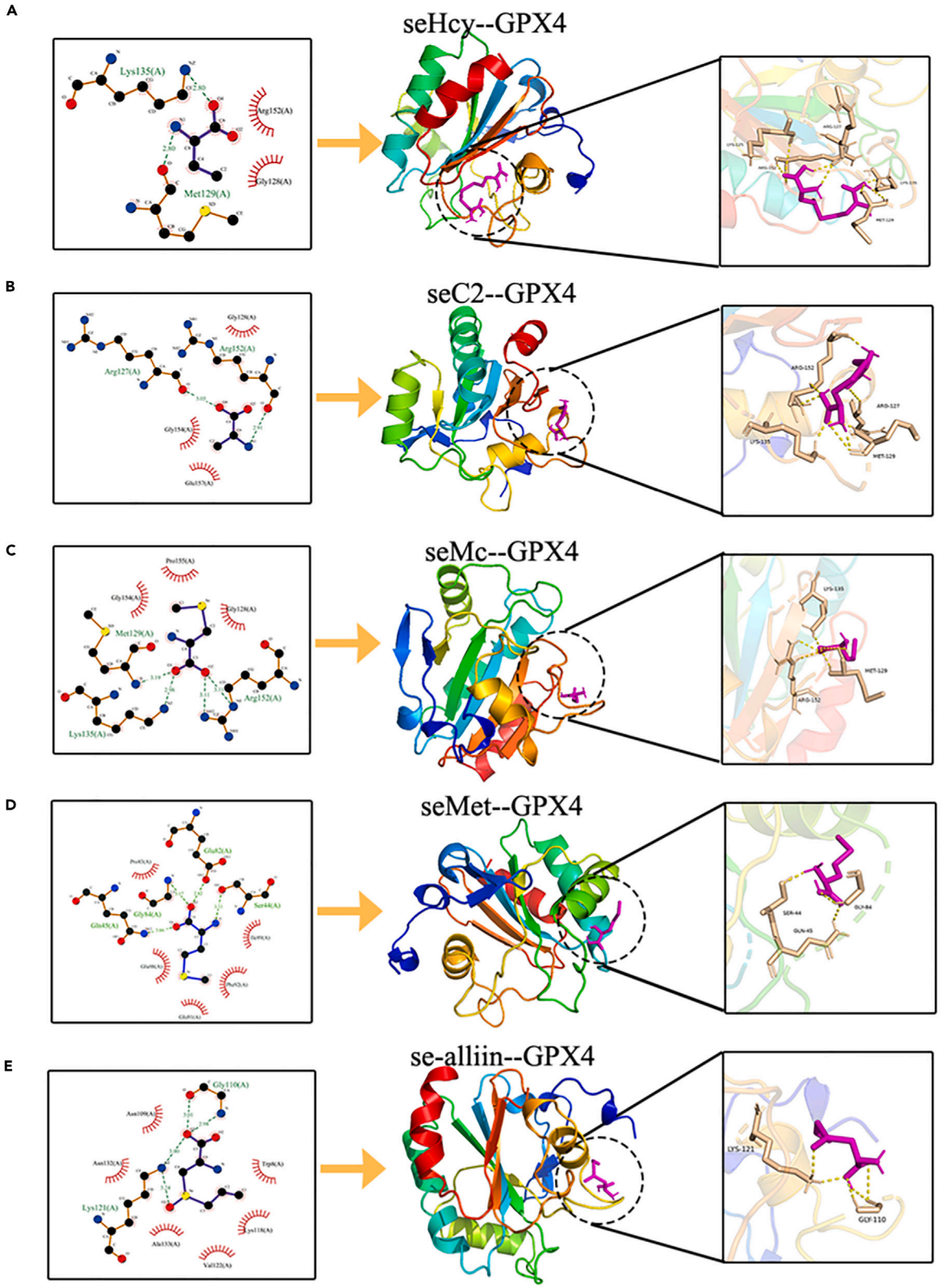
A
seHcy--GPX4
Lys135(A)
Arg152(A)
Gly128(A)
Met129(A)
B
seC2--GPX4
Gly128(A)
Arg152(A)
Arg127(A)
Gly154(A)
Glu157(A)
C
seMc--GPX4
Pro155(A)
Gly154(A)
Gly128(A)
Met129(A)
Arg152(A)
Lys135(A)
D
seMet--GPX4
Glu42(A)
Pro43(A)
Ser44(A)
Gly84(A)
Glu45(A)
E
se-alliin--GPX4
Gly110(A)
Asn109(A)
Asn132(A)
Trp9(A)
Lys121(A)
Tyr118(A)
Ala133(A)
Val122(A)

Figure 3. Molecular docking results of seleno-amino acids and GPX4 protein targets

(A) three-dimensional and two-dimensional molecular docking images of seHcy and GPX4 bonded through hydrogen bonds; (B) three-dimensional and two-dimensional molecular docking images of seC2 and GPX4 bonded through hydrogen bonds; (C) three-dimensional and two-dimensional molecular docking images of seMc and GPX4 bonded through hydrogen bonds; (D) three-dimensional and two-dimensional molecular docking images of seMet and GPX4 bonded through hydrogen bonds; (E) three-dimensional and two-dimensional molecular docking images of se-alliin and GPX4 bonded through hydrogen bonds.

seMc reduces ferroptosis and inflammation in IBD mouse models

seMc protects the intestinal barrier by reducing epithelial cell death via ferroptosis inhibition; thus, we explored how about seMc treatment with total enteral nutrition (TEN) affects IBD progression *in vitro* (Figure 6A). The body weight of the TEN intervention group decreased by 98.3% compared with the initial body weight on the fifth day of intervention, and the *p* value was less than 0.001 compared with the mean value of the control group. However, the body weight of TEN + seMc group decreased in the first 3 days, then increased on the 4th day, and the body weight of Ten + semC group was 102.4% of the initial body weight on the 7th day, which was still different from the control group, but significantly higher than DSS group (Figure 6B). Furthermore, the colon length of DSS group mice were significantly shortened to 4.96 $\pm$ 0.12 cm, which indicated that the colon appeared inflammatory injury leading to colon contracture. The colon length of TEN-treated mice recovered to 7.08 $\pm$ 0.29 cm, which was still statistically different from that of the control group (7.94 $\pm$ 0.11 cm). The colon length of TEN combined with seMc treatment group was 8.26 $\pm$ 0.61, which recovered to the level of control group (Figures 6C and 6G). And the DAI index in mice induced by DSS intervention exhibited an increment proportional to the duration of administration (Figure 6D). Mucosal damage, a hallmark of IBD, was also observed in the colon tissue of DSS-treated mice, but seMc + TEN ameliorated these symptoms, resulting in intact mucosal layers in the colon tissues. Compared with the control group, a large number of inflammatory cells infiltrated in the colonic mucosa of the DSS-fed group. After TEN combined with seMc treatment, the integrity of colonic epithelial mucosa was restored to a certain extent, and the immune and inflammatory infiltration of submucosa was reduced (Figure 6E). Consistent with the clinical sample IHC results, GPX4 expression in the colon tissues was lower in DSS group than in the control group but higher in the seMC + TEN group than in the DSS group (Figures 6F and 6G).

Since downregulated GPX4 is a key characteristic of ferroptosis, we investigated GSH and GSSG concentrations in the DSS-induced IBD mouse model. The experimental results showed that compared with the control group (10.62 $\pm$ 0.93μmol/gprot), the GSH concentration in the colon tissue of DSS-induced mice decreased (5.56 $\pm$ 0.86μmol/gprot). Compared with the DSS intervention group, the GSH concentration in the TEN treatment group and the TEN combined with seMc treatment group increased (7.72 $\pm$ 0.91μmol/gprot; 10.41 $\pm$ 0.95μmol/gprot) (Figure 6H). The difference in the increase of GSH in the colon tissue of mice after TEN combined with seMc treatment was statistically significant compared with that after TEN-treated alone (Figure 6H). The results of GSSG measurement showed no significant difference in the change of GSSG level between every group (Figure 6I). However, the GSH/GSSG ratio decreased significantly after DSS treatment, which was alleviated by TEN combined with seMc treatment (Figure 6J). The change of GSH/GSSG ratio suggested that seMc as a supplementary agent of enteral nutrition improved the antioxidant capacity of epithelial barrier in the treatment of IBD.

MDA, a lipid peroxidation marker closely related to iron death, is one of the important indicators to measure the degree of oxidative damage in the body. Therefore, we used an MDA detection kit to detect the MDA concentration in the colon tissue, and found that compared with the control group, the MDA level in the colon tissue of mice fed with DSS was significantly increased. After TEN combined with seMc treatment, the MDA level in the colon tissue of mice was reduced (Figure 6K). Since colonic epithelial cell damage aggravates inflammatory cell infiltration, we examined whether seMc could improve immune cell infiltration in colon tissues. Compared to the control group, the infiltration of T cells was observed at a proportion of 29.9%. In the TEN treatment group, this proportion increased to 39.7%, while in the TEN combined with seMc treatment group, it decreased slightly to 37.0% (Figures S4A and S4D). The control group exhibited a proportion of neutrophils at 25.5%, which significantly increased to 60.8% after DSS feeding. However, after enteral nutrition treatment, this proportion decreased to 37.8%. In the TEN combined with seMc treatment group, there was a further reduction in neutrophil proportions (35.5%), although no significant difference was observed compared to single TEN treatment alone (Figures S4B and S4D). Macrophage infiltration was also influenced by seMc treatment; initially observed at a proportion of 3.16% in the control group, it significantly increased to 17.6% in the DSS induction group and reached proportions of 5.52% and 7.63% in the TEN and TEN combined with seMc treatment groups, respectively (Figures S4C and S4D).

seMc biosafety evaluations

To examine the *in vitro* cytotoxicity of seMc, human colon epithelium-derived cells Caco-2, HCT116, and mouse macrophages (RAW 264.7) cells were incubated with different seMc concentrations for 24 h. The highest concentration of seMc (200 μg/mL) did not affect Caco-2, HCT116, and RAW 264.7 cell survival (Figures 7A–7C). To evaluate the *in vivo* toxicity of seMc, 1 mg/kg/day of seMc was administered to the mice by gavage for seven days. On the seventh day, the mice were sacrificed, and the internal organs and venous blood were collected. Evident heart, lung, liver, and kidney lesions were not observed (Figure 7D). Furthermore, the colon tissue was intact, and mucosal damage and hyperplasia were not observed in the seMc treatment group (Figure 7D). Moreover, seMc treatment did not affect the red and white blood cell counts or the hemoglobin, hematocrit, and mean corpuscular hemoglobin concentrations (Figure 7E), indicating that seMc did not produce hematological toxicity. In addition, the creatinine, blood urea nitrogen, aspartate transaminase, alanine transaminase, and creatine/blood urea nitrogen ratio values were within normal ranges, indicating that seMc did not elicit adverse effects on liver and kidney function.

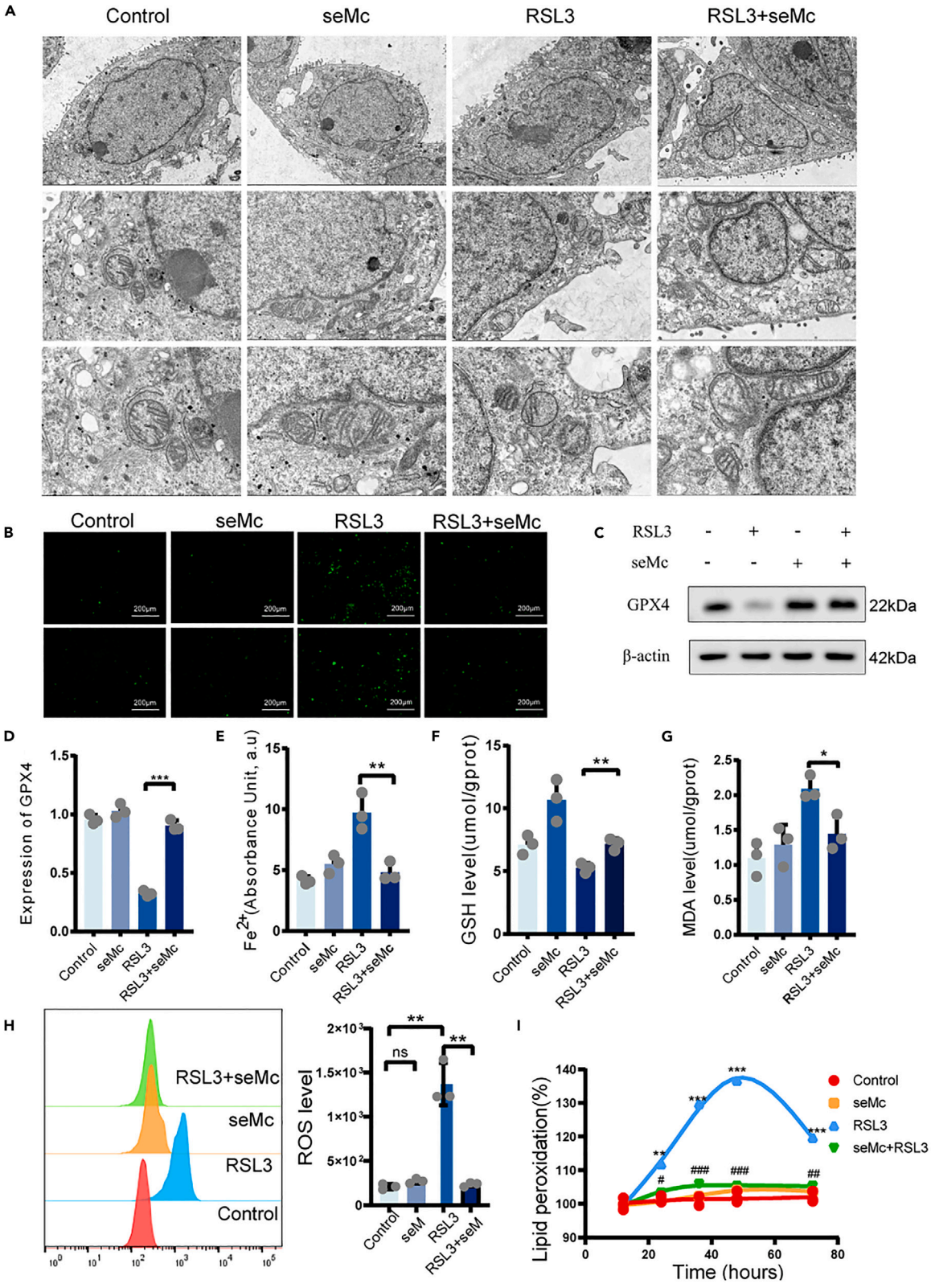
A
Control
seMc
RSL3
RSL3+seMc
B
Control
seMc
RSL3
RSL3+seMc
200μm
C
RSL3 - + - +
seMc - - + +
GPX4
22kDa
β-actin
42kDa
D
Expression of GPX4
***
Control
seMc
RSL3
RSL3+seMc
E
Fe2+(Absorbance Unit, a.u)
**
F
GSH level(umol/gprot)
**
G
MDA level(umol/gprot)
*
H
RSL3+seMc
seMc
RSL3
Control
ROS level
ns
**
I
Lipid peroxidation(%)
Time (hours)
Control
seMc
RSL3
seMc+RSL3

Figure 4. seMc inhibits RSL3-induced ferroptosis in colonic epithelial cells

(A) Morphology of mitochondria in caco2 cells treated with seMc/RSL3 under electron microscope; (B) fluorescent images of Fe^{2+} in caco2 cells treated with seMc/RSL3(scale bar: 200μm); (C) expression of GPX4 in caco2 cells treated with seMc/RSL3 measured by western blot; (D) quantification of intracellular GPX4 expression levels before and after RSL3 and seMc treatment(n = 3); (E) quantification of intracellular of Fe^{2+} before and after RSL3 and seMc treatment(n = 3); (F) GSH content(n = 3); (G) MDA content(n = 3); (H) flow cytometer of caco2 cells stained with ROS before and after RSL3 and seMc treatment; (I) Caco2 cells were treated with RSL3 (10 μM) and seMc (50 μM) for different hours and the ratio of lipid peroxidation (stained with Liperfluo) was measured by flow cytometry; data are represented as mean ± SEM. *, **, and *** indicate p values less than 0.05, 0.01, and 0.001, respectively vs. Control group; #, ##, and ### indicate p values less than 0.05, 0.01, and 0.001, respectively vs. RSL3 group.

DISCUSSION

This study reports the protective effect of seleno amino acids on the intestinal epithelium during IBD. IBD is a refractory disease, and current relief mainly relies on drug therapies, including hormones, aminosalicylic acids, immunomodulators, small-molecule drugs, and surgical treatments.[23] During the progression of IBD, the detrimental cycle between malnutrition and intestinal barrier damage leads to an imbalance in multiple nutrients and trace elements, thereby affect the prognosis and life quality of patients.[24] How to repair or effectively inhibit intestinal barrier damage during inflammation is the key to terminate this vicious cycle. In previous studies of micronutrient deficiencies in IBD patients, serum selenium deficiency was found in both CD and UC patients. Selenoproteins perform important functions in the human body, the existing studies have found that selenoprotein P is decreased and GPX1 level is increased in plasma and red blood cells of patients with Crohn's disease.[25] A study from Australia found that selenoprotein S was upregulated in intestinal epithelial cells in a mouse model of spontaneous and induced intestinal inflammation, but failed to protect these cells from oxidative stress-induced cell death.[26] However, many other types of selenoproteins are lacking in studies of IBD. Our study found that GPX4 expression levels differ in the colonic epithelium of IBD patients. According to results of IHC from clinical samples and clinical disease activity assessment, we found that the GPX4 expression decreased in the colonic epithelial tissues of patients with IBD. Surprisingly, we found that the more severe the disease, the lower the GPX4 expression in the colonic epithelium. In addition, decreased GPX4 expression correlated with patient clinical indicators, including abdominal pain and hemoglobin levels. GPX4 catalyzes the reduction of oxidized biolipids, which compensates for lipid peroxidation impairment of cell function by forming cytotoxic protein adducts or disrupting cell membranes, it is also an important ferroptosis repressor protein.[27,28] These findings provide evidence that ferroptosis is present in the epithelial barrier of IBD and is involved in the regulation of IBD disease progression. Ferroptosis of intestinal epithelial cells has been studied for a long time in gastrointestinal diseases. Ferroptosis in intestinal diseases has been studied for a long time.[29] Previous studies have found that intestinal epithelial ferroptosis is an important factor in intestinal barrier damage in IBD.[27,30–32]

GPX4, a member of the GPX family, is a selenoprotein with irreplaceable enzymatic activity.[33] Selenoproteins are proteins incorporated with selenoamino acids in peptide chains, and their synthesis is dependent on Se levels in the cell. Previous studies have found that Se deficiency exists in patients with IBD, even during remission.[34,35] Many animal experiments have demonstrated that appropriate supplementation with organic Se significantly regulating GPX4 activity,[36] minimizing the LPS-induced inflammatory response and endoplasmic reticulum stress.[37] However, a comparison among different seleno-amino acids, their effects on ferroptosis, and their functional incorporation into selenoproteins had not yet been performed. We demonstrated that five seleno-amino acids have varying protective effects against ferroptosis in an RSL3-induced IEC model; seMc had the most significant effects. We found that seleno-amino acids may not only act as direct oxidants to exert antioxidant effects, but also act as Se sources for selenoproteins and participate in the regulation of ferroptosis. We demonstrated that five seleno-amino acids have varying protective effects against ferroptosis in an RSL3-induced IEC model; seMc had the most significant effects. At pharmaco-therapeutically effective concentrations (e.g., 50 μM), seMc protected against ferroptosis and inhibited RSL3-promoted cell death, suggesting that seMc's mechanisms are likely GPX4-dependent, which inhibits lipid peroxidation damage, thereby protecting the intestinal barrier. Furthermore, we found that seMc alleviated mitochondrial atrophy and mitochondrial ridge reduction in RSL3-induced cells, key features of ferroptosis.[11,12] We have identified the expression levels of factors involved in ferroptosis and found that seMc inhibited RSL3-induced activation of NRF2/GPX4 pathways, thereby preventing ferroptosis. NRF2 is a key regulator of the cellular antioxidant response, controlling the expression of genes that counteract oxidative and electrophilic stresses, which are key factors in lipid peroxidation and ferroptosis.[38] Previous studies reported that NRF2 transcriptionally regulates GPX4 activity.[39] The Kelch-like ECH-associated protein 1 (Keap1)/Nrf2 pathway is one of the most important antioxidant defense systems in tissues and cells as it regulates the gene and protein expression of antioxidant enzymes.[40] Under normal physiological conditions, NRF2 binds to keap1 and its expression is maintained at a low level. Upon stimulation, NRF2 dissociates and activates downstream pathways to inhibit ROS production. *In vitro*, we found that the seMc promotes the expression of NRF2 and inhibits the production of ROS.[41] However, we observed decreased HO-1 expression in cells induced by LPS and RSL3. Currently, the function of HO-1 inferroptosis is still controversial. Previous study shows that overexpression of HO-1 can exacerbate ferroptosis and cause organ failure.[42] However, Previous study shows that increased HO-1 expression can protect cells from ferroptosis by inhibiting oxidative stress.[43] Our data suggest that seMc inhibits lipid peroxidation by increasing GPX4 to promote GSH synthesis, thereby protecting cells from ferroptosis, and plays an antioxidant role to prevent further cell damage by scavenging ROS, but does not for sure whether it act through activation of the NRF2/HO-1 pathway.

The significance of micronutrient supplementation in the clinical management of IBD has been consistently emphasized in recent years. Micronutrients exert a therapeutic impact on IBD by modulating immune response and programmed cell death, while insufficiency of micronutrients may also exacerbate the progression of IBD. Based on research on the antioxidant effects of se, se supplementation is considered to

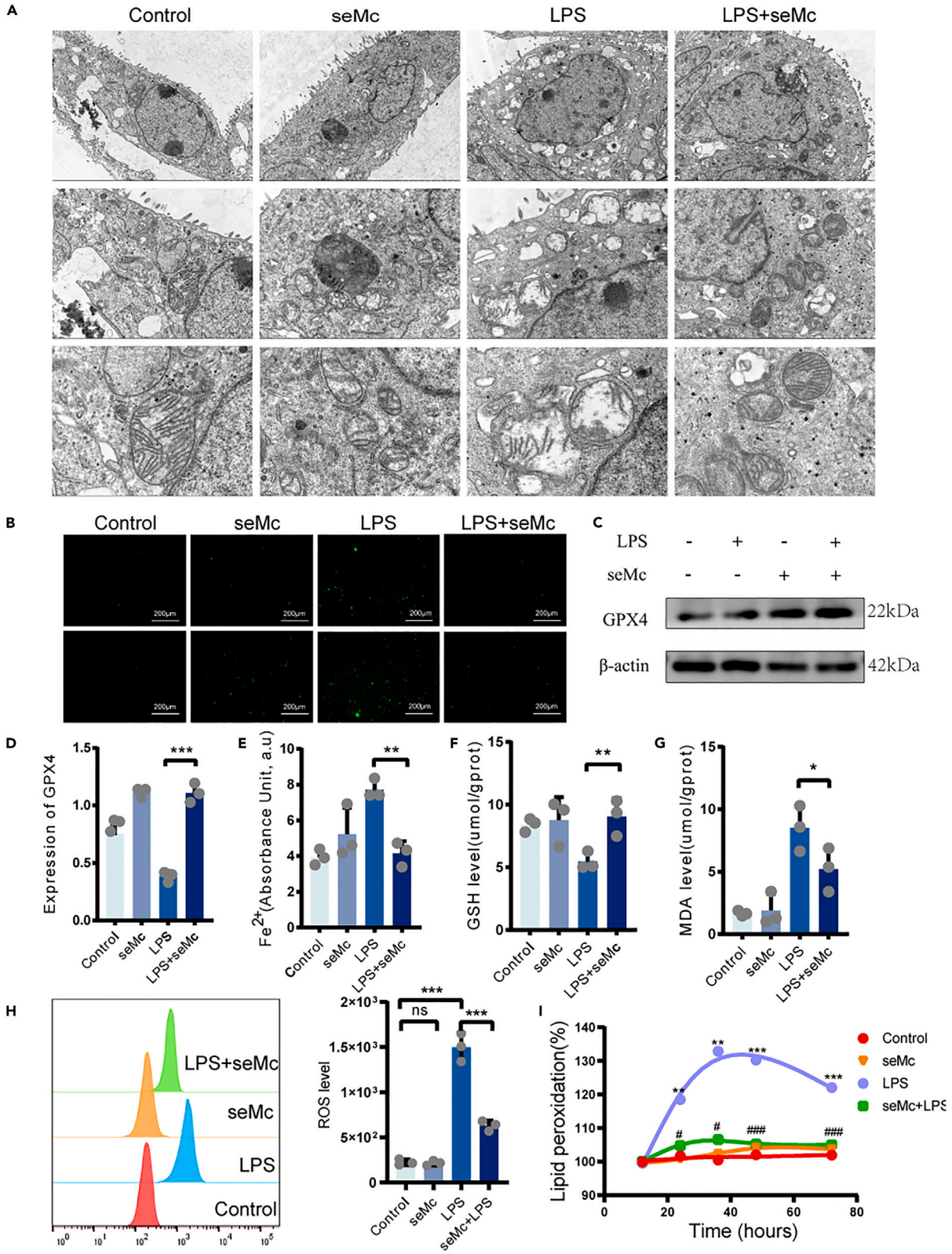
A
Control
seMc
LPS
LPS+seMc
B
Control
seMc
LPS
LPS+seMc
200μm
C
LPS - + - +
seMc - - + +
GPX4
22kDa
β-actin
42kDa
D
Expression of GPX4
***
Control
seMc
LPS
LPS+seMc
E
Fe2+(Absorbance Unit, a.u)
**
F
GSH level(umol/gprot)
**
G
MDA level(umol/gprot)
*
H
LPS+seMc
seMc
LPS
Control
ROS level
ns
***
seMc+LPS
I
Lipid peroxidation(%)
Time (hours)
Control
seMc
LPS
seMc+LPS

Figure 5. seMc inhibits LPS-induced ferroptosis in colonic epithelial cells

(A) Morphology of mitochondria in caco2 cells treated with seMc/LPS under electron microscope; (B) fluorescent images of Fe^{2+} in caco2 cells treated with seMc/LPS(scale bar: 200μm); (C) expression of GPX4 in caco2 cells treated with seMc/LPS measured by western blot; (D) quantification of intracellular GPX4 expression levels before and after LPS and seMc treatment(n = 3); (E) quantification of intracellular of Fe^{2+} before and after LPS and seMc treatment(n = 3); (F) GSH content(n = 3); (G) MDA content(n = 3); (H) flow cytometer of caco2 cells stained with ROS before and after LPS and seMc treatment; (I) Caco2 cells were treated with LPS (10 μM) and seMc (50 μM) for different hours and the ratio of lipid peroxidation (stained with Liperfluo) was measured by flow cytometry; data are represented as mean ± SEM; *, **, and *** indicate p values less than 0.05, 0.01, and 0.001, respectively vs. Control group; #, ##, and ### indicate p values less than 0.05, 0.01, and 0.001, respectively vs. LPS group.

have inhibitory effects on the development of intestinal inflammation. Previous studies have demonstrated that sodium selenite, an inorganic se supplement, can mitigate DSS-induced colitis in mice and protect the integrity of the intestinal barrier.[44] Studies involving nanomaterials containing selenium have revealed that WSe2 @F127 nanozymes effectively alleviate IBD by reducing oxidative stress damage, regulating intestinal microbiota, and modulating immune barriers.[45] Se-HMPB nanozymes have been validated to restore the integrity of the intestinal barrier by inhibiting ferroptosis and T cell differentiation in UC and CD models.[46] However, inorganic se is toxic and poorly absorbed compared to organic se which is more readily assimilated and stored by tissues. To further verify the role of seMc in IBD nutritional treatment, DSS-induced IBD mice were orally administered seMc and ENT simultaneously. ENT is an important method in the treatment of IBD. At present, it can be divided into a variety of programs, including TEN, partial enteral nutrition (PEN), CD elimination diet (CDED) combined with PEN and whole diet. TEN is currently recommended as the first-line remission therapy for mild to moderate IBD. Previous clinical studies and meta-analyses have demonstrated that TEN plays an inductive role in achieving remission and promoting intestinal mucosal healing in active IBD.[47] This treatment approach is equivalent to corticosteroids but with fewer side effects, making it a viable option for maintenance therapy during the remission stage. We observed that the combination of seMc and TEN treatment regimens exhibited superior efficacy in promoting colonic mucosal healing compared to TEN treatment alone in an experimental colitis mouse model. These findings suggest the potential application of seMc as a formulation for enteral nutrition supplementation. The expression of GPX4 protein was significantly reduced in the DSS group, whereas it was significantly increased at the colon epithelial site following seMc supplementation, indicating that oral administration of seMc enhanced GPX4 protein expression in intestinal epithelial cells. Additionally, analysis of colon tissue homogenate supernatant revealed that seMc combined with TEN treatment effectively suppressed MDA production in intestinal epithelial cells compared to the DSS group while increasing reduced GSH levels. Reduced glutathione (GSH) and oxidized glutathione (GSSG) are two forms of glutathione present *in vivo*, which interconvert through the antioxidant response mediated by GPX4 and LOOH to L-OH. Depletion of GSH and dysfunction of GPX4 lead to elevated levels of lipid hydroperoxides, further exacerbating intracellular oxidative stress. As oxidative stress intensifies, GSSG production increases, resulting in a decreased GSH/GSSG ratio indicative of an imbalance in intracellular redox state. Changes in colon tissue expression levels of GSH were observed following treatment with seMc combined with TEN. While healing and relief from inflammatory symptoms were observed at the mucosal level after treatment with TEN alone, its antioxidant protection within the intestinal epithelium was not remarkable. It is evident that seMc supplementation effectively ameliorates DSS-induced redox imbalance by enhancing GPX4 expression and utilizing its catalytic activity to attenuate lipid peroxide toxicity and reduce peroxide accumulation, thereby mitigating IEC death occurrence within the intestinal barrier.[48] Previous studies also have suggested an important relationship between ferroptosis and immune cell infiltration.[41–43,49–51] The reduction of excessive immune cell infiltration can not only effectively alleviate intestinal epithelial damage in IBD but also offer a novel approach for regulating ferroptosis in IECs through seMc.

In conclusion, this study confirmed our hypothesis that seleno-amino acids play the protective effect of intestinal barrie by blocking ferroptosis of intestinal epithelial cell and regulating immune cell infiltration. We propose that seMc combined with TEN may be a new approach for nutritional therapy in IBD patients, and the dosage and proportion of Se amino acids in the formulation can be further explored.

Limitations of the study

This study demonstrates the potential of seMc as an intestinal nutritional supplement for IBD patients, highlighting its clinical significance in treating intestinal inflammation. However, certain limitations exist in this study. Firstly, it is necessary to conduct further investigations using spontaneous IBD mouse models and immunodeficient IBD mouse models to explore additional mechanisms underlying the therapeutic effects of seMc in IBD treatment, as the current experimental inflammatory animal models are limited. Secondly, a targeted lipid metabolomics analysis should be performed to elucidate the specific mechanism by which seMc protects intestinal epithelial cells. Lastly, considering seMc's high biological activity as an organic selenium compound, it exhibits promising therapeutic potential in IBD treatment, future research directions include exploring optimal therapeutic dosages and clinical applications.

STAR★METHODS

Detailed methods are provided in the online version of this paper and include the following:

- KEY RESOURCES TABLE
- RESOURCE AVAILABILITY
  - Lead contact
  - Materials availability
  - Data and code availability
- EXPERIMENTAL MODEL AND STUDY PARTICIPANT DETAILS

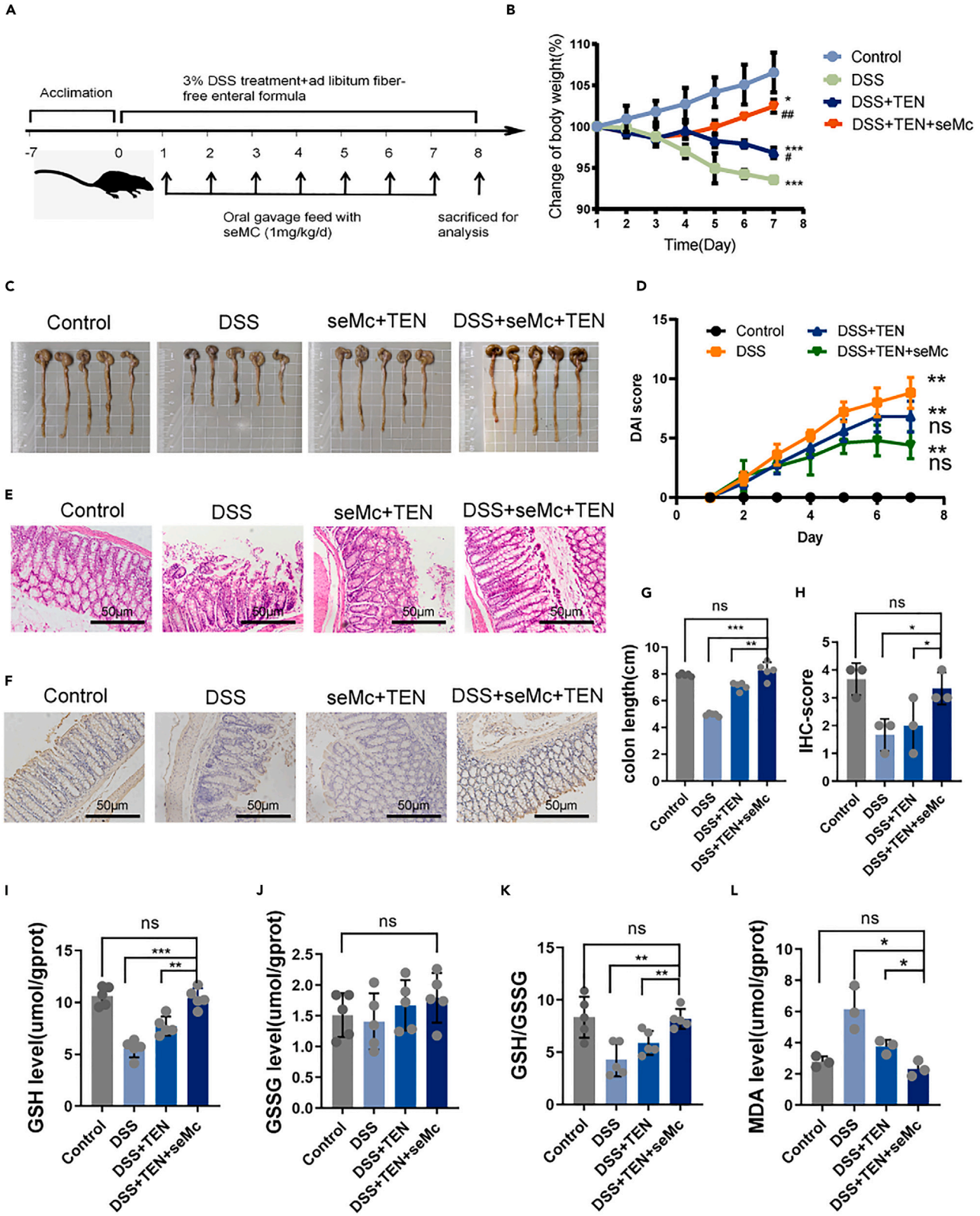
A
Acclimation
3% DSS treatment+ad libitum fiber-free enteral formula
-7
0
1
2
3
4
5
6
7
8
Oral gavage feed with seMC (1mg/kg/d)
sacrificed for analysis
B
Change of body weight(%)
Time(Day)
Control
DSS
DSS+TEN
DSS+TEN+seMc
C
Control
DSS
seMc+TEN
DSS+seMc+TEN
D
DAI score
Day
Control
DSS
DSS+TEN
DSS+TEN+seMc
E
Control
DSS
seMc+TEN
DSS+seMc+TEN
50μm
F
Control
DSS
seMc+TEN
DSS+seMc+TEN
50μm
G
colon length(cm)
ns
Control
DSS
DSS+TEN
DSS+TEN+seMc
H
IHC-score
ns
I
GSH level(umol/gprot)
ns
J
GSSG level(umol/gprot)
ns
K
GSH/GSSG
ns
L
MDA level(umol/gprot)
ns

Figure 6. seMc reduced ferroptosis and inflammation in IBD models

(A) Schematic diagram of IBD induction and seMc combined TEN treatment; (B) percentage of body weight changes of mice in different groups; (C) images of gross specimens of the colon; (D) DAI score; (E) H&E stain of colon tissue in different groups (scale bar:50 μm); (F) IHC stain images of GPX4 expression in different group (scale bar:50 μm); (G) quantification of colon length in different groups; (H) histological score of GPX4 expression in different groups; (I) level of GSH in colons from mice in different groups; (J) level GSSG in colons from mice in different groups; (K) level of GSH/GSSG in colons from mice in different groups; (L) MDA level of colon tissues from mice in different groups; data are represented as mean ± SEM; *, **, and *** indicate *p* values less than 0.05, 0.01, and 0.001, respectively vs. Control group; #, ##, and ### indicate *p*-values less than 0.05, 0.01, and 0.001, respectively vs. DSS group.

SUPPLEMENTAL INFORMATION

Supplemental information can be found online at https://doi.org/10.1016/j.isci.2024.110494.

ACKNOWLEDGMENTS

This study was financially supported by the Fundamental Research Funds for the Central Universities (11622317), National Natural Science Foundation of China (82204436), Natural Science Foundation of Guangdong Province (2022A1515011695), Guangzhou Science and Technology Plan City-School Joint Funding Project (202201020084).

AUTHOR CONTRIBUTIONS

H.F.S.C., H.J.S., and L.J. conducted the experiments and wrote the paper; Z.H. and J.H.P. contributed to the revision of the paper; P.J.H. and Z.J.; designed the experiments and revised the paper.

DECLARATION OF INTERESTS

The authors declare no competing interests.

Received: February 20, 2024
Revised: April 23, 2024
Accepted: July 9, 2024
Published: July 14, 2024

REFERENCES

1. Hodson, R. (2016). Inflammatory bowel disease. Nature *540*, S97. https://doi.org/10.1038/540S97a.
2. Schuetz, P., Seres, D., Lobo, D.N., Gomes, F., Kaegi-Braun, N., and Stanga, Z. (2021). Management of disease-related malnutrition for patients being treated in hospital. Lancet *398*, 1927–1938. https://doi.org/10.1016/S0140-6736(21)01451-3.
3. Mijac, D.D., Jankovic, G.L., Jorga, J., and Krstic, M.N. (2010). Nutritional status in patients with active inflammatory bowel disease: prevalence of malnutrition and methods for routine nutritional assessment. Eur. J. Intern. Med. *21*, 315–319. https://doi.org/10.1016/j.ejim.2010.04.012.
4. Scaldaferri, F., Pizzoferrato, M., Lopetuso, L.R., Musca, T., Ingravalle, F., Sicignano, L.L., Mentella, M., Miggiano, G., Mele, M.C., Gaetani, E., et al. (2017). Nutrition and IBD: Malnutrition and/or Sarcopenia? A Practical Guide. Gastroenterol. Res. Pract. *2017*, 8646495. https://doi.org/10.1155/2017/8646495.
5. Takaoka, A., Sasaki, M., Nakanishi, N., Kurihara, M., Ohi, A., Bamba, S., and Andoh, A. (2017). Nutritional Screening and Clinical

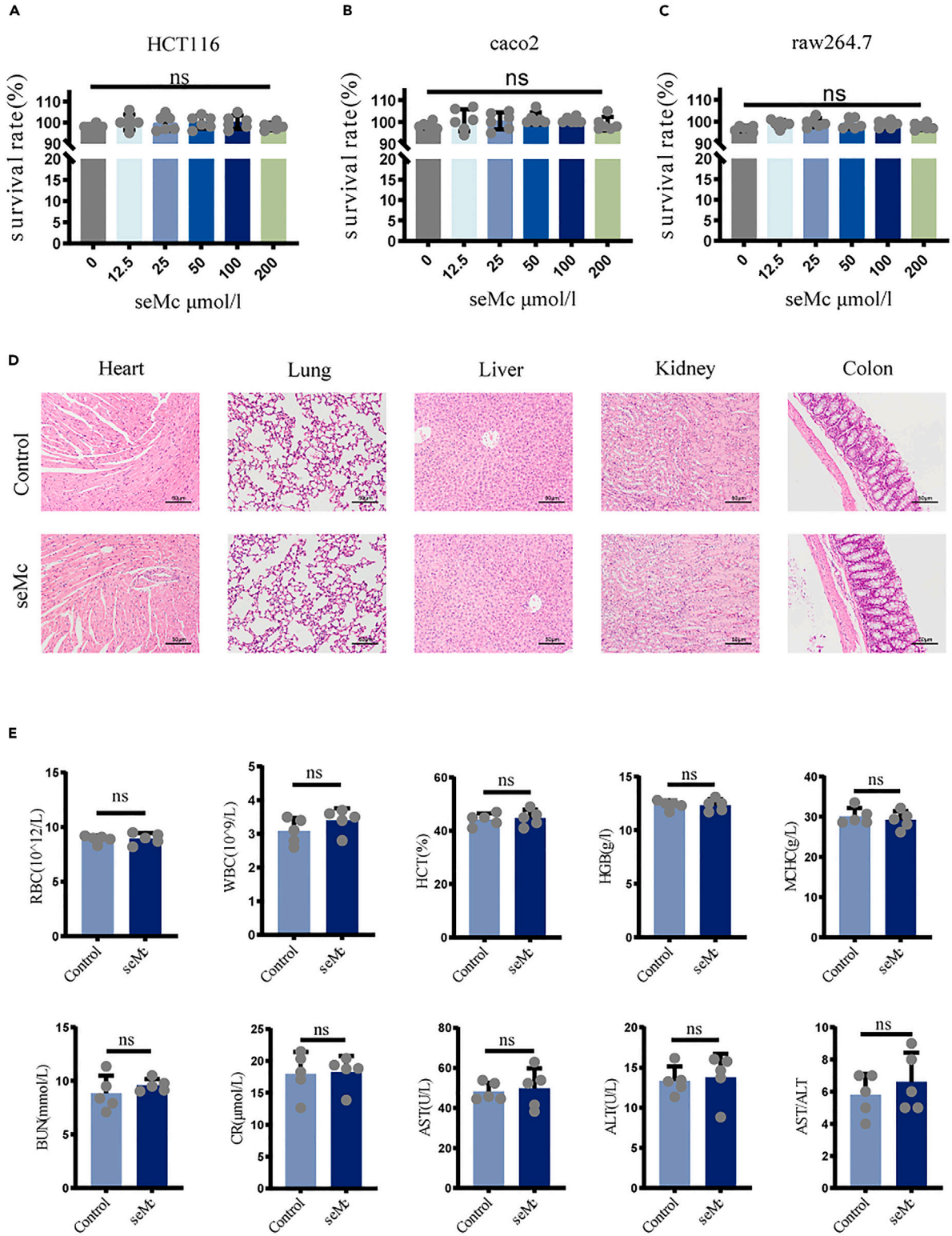

Figure 7. Biosafety evaluation of seMc

(A–C) Cell viability after seMc treatment in different cell lines.

(D) H&E stain of major organs of normal mice and seMc treated mice (Scale bar: 200 μm).

(E) Values of blood parameters and liver and kidney function indicators in normal mice (control) and POM treated mice; data are represented as mean ± SEM.

Outcome in Hospitalized Patients with Crohn's Disease. Ann. Nutr. Metab. *71*, 266–272. https://doi.org/10.1159/000485637.
6. Massironi, S., Vigano, C., Palermo, A., Pirola, L., Mulinacci, G., Allocca, M., Peyrin-Biroulet, L., and Danese, S. (2023). Inflammation and malnutrition in inflammatory bowel disease. Lancet Gastroenterol. Hepatol. *8*, 579–590. https://doi.org/10.1016/S2468-1253(23)00011-0.
7. Groschwitz, K.R., and Hogan, S.P. (2009). Intestinal barrier function: molecular regulation and disease pathogenesis. J. Allergy Clin. Immunol. *124*, 3–22. https://doi.org/10.1016/j.jaci.2009.05.038.
8. Miner-Williams, W.M., and Moughan, P.J. (2016). Intestinal barrier dysfunction: implications for chronic inflammatory conditions of the bowel. Nutr. Res. Rev. *29*, 40–59. https://doi.org/10.1017/S0954422416000019.
9. Mates, J.M., Segura, J.A., Alonso, F.J., and Marquez, J. (2010). Roles of dioxins and heavy metals in cancer and neurological diseases using ROS-mediated mechanisms. Free Radic. Biol. Med. *49*, 1328–1341. https://doi.org/10.1016/j.freeradbiomed.2010.07.028.
10. Xu, M., Tao, J., Yang, Y., Tan, S., Liu, H., Jiang, J., Zheng, F., and Wu, B. (2020). Ferroptosis involves in intestinal epithelial cell death in ulcerative colitis. Cell Death Dis. *11*, 86. https://doi.org/10.1038/s41419-020-2299-1.
11. Dixon, S.J., Lemberg, K.M., Lamprecht, M.R., Skouta, R., Zaitsev, E.M., Gleason, C.E., Patel, D.N., Bauer, A.J., Cantley, A.M., Yang, W.S., et al. (2012). Ferroptosis: an iron-dependent form of nonapoptotic cell death. Cell *149*, 1060–1072. https://doi.org/10.1016/j.cell.2012.03.042.
12. Xie, Y., Hou, W., Song, X., Yu, Y., Huang, J., Sun, X., Kang, R., and Tang, D. (2016). Ferroptosis: process and function. Cell Death Differ. *23*, 369–379. https://doi.org/10.1038/cdd.2015.158.
13. Minaiyan, M., Mostaghel, E., and Mahzouni, P. (2012). Preventive Therapy of Experimental Colitis with Selected iron Chelators and Anti-oxidants. Int. J. Prev. Med. *3*, S162–S169.
14. Werner, T., Wagner, S.J., Martinez, I., Walter, J., Chang, J.S., Clavel, T., Kisling, S., Schuemann, K., and Haller, D. (2011). Depletion of luminal iron alters the gut microbiota and prevents Crohn's disease-like ileitis. Gut *60*, 325–333. https://doi.org/10.1136/gut.2010.216929.
15. Carrier, J.C., Aghdassi, E., Jeejeebhoy, K., and Allard, J.P. (2006). Exacerbation of dextran sulfate sodium-induced colitis by dietary iron supplementation: role of NF-kappaB. Int. J. Colorectal Dis. *21*, 381–387. https://doi.org/10.1007/s00384-005-0011-7.
16. Wang, S., Liu, W., Wang, J., and Bai, X. (2020). Curculigoside inhibits ferroptosis in ulcerative colitis through the induction of GPX4. Life Sci. *259*, 118356. https://doi.org/10.1016/j.lfs.2020.118356.
17. Xu, S., He, Y., Lin, L., Chen, P., Chen, M., and Zhang, S. (2021). The emerging role of ferroptosis in intestinal disease. Cell Death Dis. *12*, 289. https://doi.org/10.1038/s41419-021-03559-1.
18. Jiang, X., Stockwell, B.R., and Conrad, M. (2021). Ferroptosis: mechanisms, biology and role in disease. Nat. Rev. Mol. Cell Biol. *22*, 266–282. https://doi.org/10.1038/s41580-020-00324-8.
19. Hariharan, S., and Dharmaraj, S. (2020). Selenium and selenoproteins: it's role in regulation of inflammation. Inflammopharmacology *28*, 667–695. https://doi.org/10.1007/s10787-020-00690-x.
20. Zhang, X., He, H., Xiang, J., Yin, H., and Hou, T. (2020). Selenium-Containing Proteins/Peptides from Plants: A Review on the Structures and Functions. J. Agric. Food Chem. *68*, 15061–15073. https://doi.org/10.1021/acs.jafc.0c05594.
21. Short, S.P., Pilat, J.M., Barrett, C.W., Reddy, V.K., Haberman, Y., Hendren, J.R., Marsh, B.J., Keating, C.E., Motley, A.K., Hill, K.E., et al. (2021). Colonic Epithelial-Derived Selenoprotein P Is the Source for Antioxidant-Mediated Protection in Colitis-Associated Cancer. Gastroenterology *160*, 1694–1708.e3. https://doi.org/10.1053/j.gastro.2020.12.059.
22. Gordon, H., Biancone, L., Fiorino, G., Katsanos, K.H., Kopylov, U., Al, S.E., Axelrad, J.E., Balendran, K., Burisch, J., de Ridder, L., et al. (2023). ECCO Guidelines on Inflammatory Bowel Disease and Malignancies. J. Crohns Colitis *17*, 827–854. https://doi.org/10.1093/ecco-jcc/jjac187.
23. Elhag, D.A., Kumar, M., Saadaoui, M., Akobeng, A.K., Al-Mudahka, F., Elawad, M., and Al, K.S. (2022). Inflammatory Bowel Disease Treatments and Predictive Biomarkers of Therapeutic Response. Int. J. Mol. Sci. *23*, 6966. https://doi.org/10.3390/ijms23136966.
24. Pulley, J., Todd, A., Flatley, C., and Begun, J. (2020). Malnutrition and quality of life among adult inflammatory bowel disease patients. JGH Open *4*, 454–460. https://doi.org/10.1002/jgh3.12278.
25. Barros, S., Dias, T., Moura, M., Soares, N., Pierote, N., Araujo, C., Maia, C., Henriques, G.S., Barros, V.C., Moita Neto, J.M., et al. (2020). Relationship between selenium status and biomarkers of oxidative stress in Crohn's disease. Nutrition *74*, 110762. https://doi.org/10.1016/j.nut.2020.110762.
26. Speckmann, B., Gerloff, K., Simms, L., Oancea, I., Shi, W., McGuckin, M.A., Radford-Smith, G., and Khanna, K.K. (2014). Selenoprotein S is a marker but not a regulator of endoplasmic reticulum stress in intestinal epithelial cells. Free Radic. Biol. Med. *67*, 265–277. https://doi.org/10.1016/j.freeradbiomed.2013.11.001.
27. Mayr, L., Grabherr, F., Schwarzler, J., Reitmeier, I., Sommer, F., Gehmacher, T., Niederreiter, L., He, G.W., Ruder, B., Kunz, K.T.R., et al. (2020). Dietary lipids fuel GPX4-restricted enteritis resembling Crohn's disease. Nat. Commun. *11*, 1775. https://doi.org/10.1038/s41467-020-15646-6.
28. Stockwell, B.R., Friedmann, A.J., Bayir, H., Bush, A.I., Conrad, M., Dixon, S.J., Fulda, S., Gascón, S., Hatzios, S.K., Kagan, V.E., et al. (2017). Ferroptosis: A Regulated Cell Death Nexus Linking Metabolism, Redox Biology, and Disease. Cell *171*, 273–285. https://doi.org/10.1016/j.cell.2017.09.021.
29. Xu, C., Liu, Z., and Xiao, J. (2021). Ferroptosis: A Double-Edged Sword in Gastrointestinal Disease. Int. J. Mol. Sci. *22*, 12403. https://doi.org/10.3390/ijms222212403.
30. Huang, J., Zhang, J., Ma, J., Ma, J., Liu, J., Wang, F., and Tang, X. (2022). Inhibiting Ferroptosis: A Novel Approach for Ulcerative Colitis Therapeutics. Oxid. Med. Cell. Longev. *2022*, 9678625. https://doi.org/10.1155/2022/9678625.
31. Wei, Z., Hang, S., Wiredu, O.D., Zhang, Z., Wang, B., Zhang, X., and Mao, F. (2023). Human umbilical cord mesenchymal stem cells derived exosome shuttling mir-129-5p attenuates inflammatory bowel disease by inhibiting ferroptosis. J. Nanobiotechnology *21*, 188. https://doi.org/10.1186/s12951-023-01951-x.
32. Wu, Y., Ran, L., Yang, Y., Gao, X., Peng, M., Liu, S., Sun, L., Wan, J., Wang, Y., Yang, K., et al. (2023). Deferasirox alleviates DSS-induced ulcerative colitis in mice by inhibiting ferroptosis and improving intestinal microbiota. Life Sci. *314*, 121312. https://doi.org/10.1016/j.lfs.2022.121312.
33. Pei, J., Pan, X., Wei, G., and Hua, Y. (2023). Research progress of glutathione peroxidase family (GPX) in redoxidation. Front. Pharmacol. *14*, 1147414. https://doi.org/10.3389/fphar.2023.1147414.
34. Hu, R., Xiao, J., and Fan, L. (2024). The Role of the Trace Element Selenium in Inflammatory Bowel Disease. Biol. Trace Elem. Res. https://doi.org/10.1007/s12011-024-04074-y.
35. Kudva, A.K., Shay, A.E., and Prabhu, K.S. (2015). Selenium and inflammatory bowel disease. Am. J. Physiol. Gastrointest. Liver Physiol. *309*, G71–G77. https://doi.org/10.1152/ajpgi.00379.2014.
36. Friedmann, A.J., and Conrad, M. (2018). Selenium and GPX4, a vital symbiosis. Free Radic. Biol. Med. *127*, 153–159. https://doi.org/10.1016/j.freeradbiomed.2018.03.001.
37. Shi, C., Yue, F., Shi, F., Qin, Q., Wang, L., Wang, G., Mu, L., Liu, D., Li, Y., Yu, T., and She, J. (2021). Selenium-Containing Amino Acids Protect Dextran Sulfate Sodium-Induced Colitis via Ameliorating Oxidative Stress and Intestinal Inflammation. J. Inflamm. Res. *14*, 85–95. https://doi.org/10.2147/JIR.S288412.
38. Dodson, M., Castro-Portuguez, R., and Zhang, D.D. (2019). NRF2 plays a critical role in mitigating lipid peroxidation and ferroptosis. Redox Biol. *23*, 101107. https://doi.org/10.1016/j.redox.2019.101107.
39. Lei, G., Mao, C., Yan, Y., Zhuang, L., and Gan, B. (2021). Ferroptosis, radiotherapy, and combination therapeutic strategies. Protein Cell *12*, 836–857. https://doi.org/10.1007/s13238-021-00841-y.
40. Yamamoto, M., Kensler, T.W., and Motohashi, H. (2018). The KEAP1-NRF2 System: a Thiol-Based Sensor-Effector Apparatus for Maintaining Redox Homeostasis. Physiol. Rev. *98*, 1169–1203. https://doi.org/10.1152/physrev.00023.2017.
41. Wang, P., and Lu, Y.Q. (2022). Ferroptosis: A Critical Moderator in the Life Cycle of Immune Cells. Front. Immunol. *13*, 877634. https://doi.org/10.3389/fimmu.2022.877634.
42. Wu, J., Liu, Q., Zhang, X., Tan, M., Li, X., Liu, P., Wu, L., Jiao, F., Lin, Z., Wu, X., et al. (2022). The interaction between STING and NCOA4 exacerbates lethal sepsis by orchestrating ferroptosis and inflammatory responses in macrophages. Cell Death Dis. *13*, 653. https://doi.org/10.1038/s41419-022-05115-x.
43. Yang, Y., Wang, Y., Guo, L., Gao, W., Tang, T.L., and Yan, M. (2022). Interaction between macrophages and ferroptosis. Cell Death Dis. *13*, 355. https://doi.org/10.1038/s41419-022-04775-z.
44. Zhong, Y., Jin, Y., Zhang, Q., Mao, B., Tang, X., Huang, J., Guo, R., Zhao, J., Cui, S., and Chen, W. (2022). Comparison of Selenium-Enriched Lactobacillusparacasei, Selenium-Enriched Yeast, and Selenite for the Alleviation of DSS-Induced Colitis in Mice. Nutrients *14*, 2433. https://doi.org/10.3390/nu14122433.
45. Jiang, K., Cao, X., Wu, H., Xu, Y., Liu, L., Qian, H., Miao, Z., Wang, H., and Ma, Y. (2024). 2D

Nanozymes Modulate Gut Microbiota and T-Cell Differentiation for Inflammatory Bowel Disease Management. Adv. Healthc. Mater. *13*, e2302576. https://doi.org/10.1002/adhm.202302576.

46. Zhu, D., Wu, H., Jiang, K., Xu, Y., Miao, Z., Wang, H., and Ma, Y. (2023). Zero-Valence Selenium-Enriched Prussian Blue Nanozymes Reconstruct Intestinal Barrier against Inflammatory Bowel Disease via Inhibiting Ferroptosis and T Cells Differentiation. Adv. Healthc. Mater. *12*, e2203160. https://doi.org/10.1002/adhm.202203160.
47. Grover, Z., Muir, R., and Lewindon, P. (2014). Exclusive enteral nutrition induces early clinical, mucosal and transmural remission in paediatric Crohn's disease. J. Gastroenterol. *49*, 638–645. https://doi.org/10.1007/s00535-013-0815-0.
48. Micheli, L., Collodel, G., Cerretani, D., Menchiari, A., Noto, D., Signorini, C., and Moretti, E. (2019). Relationships between Ghrelin and Obestatin with MDA, Proinflammatory Cytokines, GSH/GSSG Ratio, Catalase Activity, and Semen Parameters in Infertile Patients with Leukocytospermia and Varicocele. Oxid. Med. Cell. Longev. *2019*, 7261842. https://doi.org/10.1155/2019/7261842.
49. Han, F., Li, S., Yang, Y., and Bai, Z. (2021). Interleukin-6 promotes ferroptosis in bronchial epithelial cells by inducing reactive oxygen species-dependent lipid peroxidation and disrupting iron homeostasis. Bioengineered *12*, 5279–5288. https://doi.org/10.1080/21655979.2021.1964158.
50. Handa, P., Thomas, S., Morgan-Stevenson, V., Maliken, B.D., Gochanour, E., Boukhar, S., Yeh, M.M., and Kowdley, K.V. (2019). Iron alters macrophage polarization status and leads to steatohepatitis and fibrogenesis. J. Leukoc. Biol. *105*, 1015–1026. https://doi.org/10.1002/JLB.3A0318-108R.
51. Zhou, Y., Que, K.T., Zhang, Z., Yi, Z.J., Zhao, P.X., You, Y., Gong, J.P., and Liu, Z.J. (2018). Iron overloaded polarizes macrophage to proinflammation phenotype through ROS/acetyl-p53 pathway. Cancer Med. *7*, 4012–4022. https://doi.org/10.1002/cam4.1670.
52. Tanguy, S., Grauzam, S., de Leiris, J., and Boucher, F. (2012). Impact of dietary selenium intake on cardiac health: experimental approaches and human studies. Mol. Nutr. Food Res. *56*, 1106–1121. https://doi.org/10.1002/mnfr.201100766.

STAR★METHODS

KEY RESOURCES TABLE

REAGENT or RESOURCE	SOURCE	IDENTIFIER
Antibodies		
GPX4	Beyotime	#AF7020
NRF2	SAB	#41255
HO-1	proteintech	#10701-1-AP
HRP-conjugated Affinipure Goat Anti-Mouse IgG	proteintech	#SA00001-1-100UL
HRP-conjugated Affinipure Goat Anti-Rabbit IgG	proteintech	#SA00001-2-100ul
F4/80 clone BM8 PE/Cyanine5	BioLegend	N/A
Ly-6G clone 1A8 APC/Fire 750	BioLegend	N/A
CD3 clone 17A2 APC	BioLegend	N/A
Biological samples		
Human colon paraffin pathological section	The First Affiliated Hospital of Jinan University	N/A
Chemicals, peptides, and recombinant proteins		
RSL3	Selleck Chemicals LLC, TX, USA	#S8155
Seleno-amino acids	Department of Food Science and Engineering of Jinan university	N/A
Critical commercial assays		
the green-fluorescent heavy metal indicator Phen Green™ SK dipotassium salt assay	Thermo Fisher	#P14312
malondialdehyde kit	Cominbio	#MDA-1-Y
BCA Protein Assay Kit	Beyotime	#P0012
GSH and GSSH assay kit	Beyotime	#P0053
Deposited data		
PDB database	5L71, PDB DOI: https://doi.org/10.2210/pdb5L71/pdb	http://www.rcsb.org/
seleno amino acids data	This paper	https://pubchem.ncbi.nlm.nih.gov/
Experimental models: Cell lines		
Caco2	the Cell Bank of the Chinese Academy of Sciences	N/A
HCT116	the Cell Bank of the Chinese Academy of Sciences	N/A
Experimental models: Organisms/strains		
Mouse: C57BL/6	Bestext Biotechnology Co. Ltd	Mouse (Mus musculus)/SPF/ C57BL/6/Sentinel mouse
Software and algorithms		
CytExpert software	Beckman Coulter, Brea, CA, USA	https://cytexpert.updatestar.com/
ImageJ	N/A	https://imagej.nih.gov/ij/
Chem 3D pro software	N/A	https://www.wavemetrics.com/project/Chem3D
AutoDock Tools(ADT, version 4.2)	N/A	https://autodock.scripps.edu/
PyMoL software (version 2.2.0)	N/A	https://github.com/schrodinger/pymol-open-source
AutoDock Vina (version 1.1.2)	O. Trott, A. J. Olson et al.	http://vina.scripps.edu

RESOURCE AVAILABILITY

Lead contact

Further information and requests for resources and reagents should be directed to and will be fulfilled by the lead contact, Prof. Jinghua Pan, (huajanve@foxmail.com).

Materials availability

This research adopts the selenium amino acid reagent synthesized from food engineering college, jinan university, the details in the Data S1 and S2.

Data and code availability

- All data reported in this paper will be shared by the lead contact upon request.
- This paper does not report original code.
- Any additional information required to reanalyze the data reported in this paper is available from the lead contact upon request.

EXPERIMENTAL MODEL AND STUDY PARTICIPANT DETAILS

Cell culture

Caco-2, HCT116, and RAW 264.7 cells were obtained from the Cell Bank of the Chinese Academy of Sciences (Shanghai, China). Cells were cultured in Dulbecco's Modified Eagle's Medium (Gibco/Thermo Fisher Scientific, Waltham, MA, USA) with 10% fetal bovine serum (Gibco) in a humidified incubator with 5% CO_2 at 37°C.

Animal model

Nine-week-old female C57BL/6 mice were purchased from Bestext Biotechnology Co. Ltd. (Nantong, China). The Fiber-free enteral nutrition formula milk powder, commonly known as Ensure Plus from Abbott Laboratories, is a widely utilized oral preparation for total enteral nutrition. Each 100g serving provides 462kcal, with protein accounting for 16%, carbohydrates accounting for 48%, and fats accounting for 36%. Twenty healthy mice were randomly divided into 4 groups, with 4 mice in each group: 1) control group (normal drinking water+normal diet); 2) 3% DSS solution (Drinking water containing 3%DSS+normal diet); 3) 3% DSS+TEN (55.8g ensure powder added to 200ml drinking water) ; 4) 3% DSS +TEN+seMc solution (1mg/kg/d).[52] Body weight was measured daily. The mice were sacrificed on the seventh day, and colon samples were taken for length measurement and hematoxylin and eosin (HE) and immunohistochemical (IHC) staining. Each mouse in the group was assessed daily based on three parameters: body weight, fecal consistency, and presence of occult blood in the feces. The Disease Activity Index (DAI) score represents the cumulative value of these three indicators.This study has been approved by the Experimental Animal Ethics Committee of Jinan University (Approval No. 102144).

Clinical samples

Paraffin-embedded sections of clinical samples were collected from our institution. We collected 30 colon tissue paraffin sections from patients diagnosed with IBD between 2013 and 2022, following the gold standard of pathology. Paraffin sections of normal colon tissues from seven patients after partial colectomy were used as the control group. The disease status was classified. Based on the clinical disease activity index (CDAI) of Crohn's disease, the patients were divided into severe group (n=5), moderate group (n=8), and mild group (n=5). Based on the modified Mayo score, the ulcerative colitis patients were divided into severe group (n=3), moderate group (n=5), and mild group (n=4). The use of clinical samples had been approved by Jinan university Medical ethics committe (Approval No. JNUKY-2023-0105).

METHOD DETAILS

Assaying cell viability with CCK8

First, 10,000 cells/well of Caco-2 and HCT116 cells were seeded into 96-well plates and grown at 37°C and 5% CO_2 for 24 h. Then, 10 μmol/L of RSL3 (Selleck Chemicals LLC, TX, USA), a ferroptosis activator, was added to the wells and incubated for 30 min, followed by treatment with 0, 12.5, 25, 50, 100, and 200 μg/mL of selenohomocysteine (seHcy), seC2, L-se-Methylselenocysteine (seMc), seMet, or selenoic-alliin (se-alliin) (provided by the School of Food Engineering, Jinan University, details in Data S1 and S2) for 24 hours. After 24 hours of seleno-amino acids treatment, the old cell culture medium was removed and replaced with 100 μL of fresh cell culture medium containing 10 μL of CCK8 reagent in each well, and then it was placed in darkness for 1.5 hours in the incubator. The absorbance at 450 nm was determined using a microplate reader.

Inductively coupled plasma-mass spectrometry (ICP-MS)

For this the cells were treated with different seleno-amino acids with 100μg/mL for 24 hours. After that the cells were lysed using lysis buffer (10 mM Tris-HCl, 150 mM NaCl, 1% Triton-X, 0.1% SDS) and then analyzed by ICP-MS. The ICP-MS analysis was performed using an Agilent

7500 Series ICP-MS instrument (Agilent Technologies Inc., Santa Clara, CA, USA) and calibration curves were prepared using Rh as internal standard. The mean of three separate replicates was used for determination of se concentration.

Intracellular mitochondrial observation experiments

Caco-2 cells were seeded onto 100-mm Petri dishes, cultivated for 24 h, then treated with RSL3 (10 μM) and seMc (50 μM) for 24 hours. The culture medium was discarded, and the cells were washed once with phosphate-buffered saline and collected by centrifugation at 1,000 rpm. The cell suspensions were prepared by adding DMEM medium and mixing. The morphology of intracellular mitochondria was observed using a projection electron microscope.

Western blot analysis

Proteins were extracted from Caco-2 cells. A BCA protein assay (Beyotime, P0012, Shanghai, China) was used to measure the protein concentration. Sodium dodecyl sulfate-polyacrylamide gel electrophoresis was used to separate proteins, which were then transferred to a polyvinylidene fluoride membrane (Merck Millipore, Burlington, MA, USA). The membranes were blocked with 5% skim milk and then incubated with primary antibodies (GPX4, Beyotime, #AF7020; NRF2, SAB, #41255; HO-1, proteintech, #10701-1-AP) at 4°C overnight. The next day, the membranes were incubated with secondary antibodies (HRP-conjugated Affinipure Goat Anti-Mouse IgG, proteintech, SA00001-1-100UL; HRP-conjugated Affinipure Goat Anti-Rabbit IgG, proteintech, SA00001-2-100ul) for 1 hour at room temperature and then imaged with an enhanced chemiluminescence reagent (Cell Signaling Technology, Danvers, MA, United States) using an imaging system (Thermo Fisher Scientific).

Iron (Fe^{2+}) assay

Fe^{2+} levels were measured using the green-fluorescent heavy metal indicator Phen Green™ SK dipotassium salt (Thermo Fisher, P14312) following the manufacturer's instructions.

Malondialdehyde (MDA) measurement

MDA content in Caco2 cells was measured by the malondialdehyde kit (Cominbio, Suzhou, China, #MDA-1-Y) according to the manufacturer's instructions. Cell were lysed with MDA extraction solution and centrifuged for 10 min at 8000×g and 4°C. The supernatant was used to measure the MDA content. The protein concentration (Cprot) was measured by BCA Protein Assay Kit (Beyotime, #P0012). The absorbances at 532 nm (A532) and 600 nm (A600) were measured by a microplate photometer. MDA content (nmol/mg protein) was calculated as follows: MDA (nmol/mg protein) = 51.6 × (A532-A600)/Cprot.

GSH levels and the GSH to glutathione disulfide (GSSG) measurement

Caco2 cells were lysed with RIPA lysis buffer and the supernatant was collected. The GSH and GSSH content in the supernatant was assessed by GSH and GSSH assay kit (Beyotime. #S0053) according to the manufacturer's instructions. The absorbance was measured at 405nm (A412).

ROS scavenge test in cells

Approximately 1×10^6 caco2 cells were seeded into a 6-well plate and treated with RSL3 and seMc for 24h. After 24 hours of seleno-amino acids treatment, the old cell culture medium was removed and replaced with DCFH-DA reagent diluted in DMEM at a concentration of 10 μmol/L in each well. As soon as incubated in incubator at 37°C for 20 minutes, cells were washed three times with serum-free cell culture medium. Cell suspensions were prepared in PBS, and the fluorescence intensity of DCF fluorescein was measured on CytoFLEX Flow Cytometer and CytExpert software, respectively (Beckman Coulter, Brea, CA, USA).

Analysis of lipid perdoxidation

Caco2 cells were dispensed in 6-well plate at a density of 1×10^6 cells. Cells received RSL3 (10 μM) for 12 h, 24h, 36h, 48h, 72h, respectively, and received seMc (50 μM) for the same time. After treatment, cells were incubated with Liperfluo (10 μM) (DOJINDO, Japan) for 1 h. Then, the cells were collected for analysis in a CytoFLEX Flow Cytometer and CytExpert software. The excitation and emission wavelengths of the oxidized Liperfluo are 488 and 535 nm, respectively.

Molecular docking

To further verify the binding ability between seleno amino acids and GPX4, molecular docking was performed. The crystal structures of GPX4 (5L71, PDB DOI: https://doi.org/10.2210/pdb5L71/pdb) were obtained from the PDB database (http://www.rcsb.org/). Using autodock tools (version 4.2) to add hydrogen to the protein, calculate the charge, and then turn it into PDBQT file. The seleno amino acids data were from (https://pubchem.ncbi.nlm.nih.gov/) database to download the sdf file. The chemical structure of seleno amino acids were mapped using Chembio ultra, used the Chem 3D pro software to calculate the minimum energy, turn into a mole, and then convert it to PDBQT. Docking studies of the core targets and binding energe were performed using AutoDock Tools (ADT, version 4.2) and AutoDock Vina (version 1.1.2). The docking results were visualized using PyMoL software (version 2.2.0).

Flow cytometry analysis

The mice were sacrificed, and the colons were harvested. After rinsing with phosphate-buffered saline, the colons were sectioned into small pieces and digested with a digestion solution containing collagenase for 30 min. After digestion, the fragments were dissociated into single-cell suspensions using a dissociator (Miltenyi Biotec, Germany) and filtered through a 70-mesh cell sieve to remove residual tissue fragments. A lysis solution (BD Biosciences, Franklin Lakes, NJ, USA) was used to remove erythrocytes. A mixture of fluorochrome-conjugated antibodies was used for fluorescence staining as follows: F4/80 clone BM8 PE/Cyanine5 (BioLegend), Ly-6G clone 1A8 APC/Fire 750 (BioLegend), and CD3 clone 17A2 APC (BioLegend). Data were collected and analyzed using a CytoFLEX Flow Cytometer and CytExpert software, respectively (Beckman Coulter, Brea, CA, USA). A sequential gating strategy was used to differentiate different cell populations.

HE staining

C57BL/6 mouse colon tissues were frozen, sliced into 5 μm-thick sections, fixed with 4% paraformaldehyde, and sequentially stained with HE to observe histological changes. The HE staining method was performed as follows: Mouse colon tissue was collected and washed with PBS, fixed in 4% formaldehyde, trimmed to approximately 1cm^2, and placed in an embedding mold to prepare paraffin sections. Subsequently, the colon tissue was soaked overnight in 70% ethanol followed by sequential transfer into 80% to 100% ethanol. After decolorization with xylene for 20 minutes, the tissue was embedded in paraffin and cut into 5 μm sections on a freezing slide. The second step involved HE staining. Paraffin sections were dewaxed by placing them in xylene for 20 minutes; then they were stained with hematoxylin for 2 minutes and counter-stained with safranin for 10 minutes, followed by eosin stain for one minute. The stained sections were dehydrated using a series of graded alcohol solutions and xylene solutions before being mounted on microscope slides using neutral resin. According to your suggestion, we have added this information to the method section.

IHC

Samples collected from the mice and patients were fixed in 4% paraformaldehyde and embedded in paraffin. The sections were deparaffinized and hydrated, followed by antigen retrieval using an ethylenediaminetetraacetic acid (i.e., EDTA) solution (pH 9.0). All sections were incubated with GPX4 antibody at 4°C overnight. The next day, the sections were incubated with a horseradish peroxidase-labeled secondary antibody. A chromogenic reaction was induced using diaminobenzidine (i.e., DAB). IHC scoring was conducted using a staining intensity method, where Image J was employed to measure the average gray value (staining intensity) and positive area percentage (staining area) of positive cells. Four scoring values were assigned: High positive (3+), Positive (2+), Low positive (1+), and Negative (0+).

QUANTIFICATION AND STATISTICAL ANALYSIS

GraphPad Prism 8.0 (GraphPad Software Inc., San Diego, CA, USA) was used for statistical analysis. Student's t-tests were used to compare two groups, and p-values of <0.05 were considered statistically significant. All bar graphs included scattered dots. All bar graphs represent mean $\pm$ SD. Parametric test were used to assum gaussian distribution and unpaired t-test were used to assume both population have the same SD. The symbols *, **, and *** indicate p-values less than 0.05, 0.01, and 0.001, respectively. Similarly, #, ##, and ### represent p-values less than 0.05, 0.01, and 0.001 correspondingly. In Figures 4I and 5I, the * symbol denotes statistical significance compared to the Control group; in Figure 4I, the # symbol represents statistical significance compared to the RSL3 group; while in Figure 5I, the * symbol indicates statistical significance compared to the Control group and the # symbol signifies statistical significance compared to the LPS group. Within the *in vivo* experiment section,* represents statistical significance compared to the Control group while # represents statistical significance compared to DSS group. Results are expressed as means +/- SEM. All quantitative experiments (western blot, cell count) included at least 3 biological replicates. Animal studies included at least 5 mice per group. The value of n number of representative samples, part of the value of n number *in vitro* experiments on behalf of the repetition of the test sample size, n value *in vivo* experiments on behalf of the number of mice. Correlation analysis used Pearson's correlation coefficient analysis to measure the linear correlation between two variables, ranging from -1 to +1, where -1 means completely negative correlation, +1 means completely positive correlation, and 0 means no linear correlation. R^2 is for correlation coefficient.

ADDITIONAL RESOURCES

Additional Substrate Preparation and 1H and 13CNMR Spectra of Products for the seleno-amino acids employed are provided in this study, and the information has been reported in Data S1 and S2.